Characterisation and simulation of the influence of propellant geometric variability on gas delivery profiles

HAD Alrashidy

orcid.org/0000-0003-4735-7499

Dissertation accepted in partial fulfilment of the requirements for the degree *Master of Science in Mechanical Engineering* at the North-West University

Supervisor: Prof WL den Heijer

Co-supervisor: Mr V Schabort

Graduation: July 2020

Student number: 24560383

ACKNOWLEDGEMENTS

I would like to express my gratitude to Prof. W. L. den Heijer and Mr. Victor Schabort for their guidance and supervision while working on this study. Their technical knowledge was shared with me with no hesitation, and I thank them for their cooperation whenever I had to face an obstacle in my way.

I would like also to thank Mr. Manie Johannes for helping me with all the experimental data collection conducted during this study. This research would also not have been possible without the financial aid from the Military Industries Corporation (MIC). Furthermore, I would like to thank Rheinmetall Denel Munition (RDM) for their logistical support, as well as the various training courses that I undertook. I further acknowledge the North-West University (NWU) for their support and academic courses.

I also wish to express my heartfelt gratitude to my wife, Amal. I still recall her struggles when she was writing her own dissertation. She gave me the inspiration for this dissertation and supported me with her patience and her incredible attitude. Also, thank you to my children for their patience and the time they spent in the background while I was studying.

Finally, many thanks to Alshehri Abdullatif for his encouragement.

ABSTRACT

Ballisticians do not currently take the significance of propellant grain geometry variance into account for the various solid propellants found within guns of various calibres (Baschung & Grüne, 2000).

Conventional Internal Ballistic (IB) simulation codes assume that the geometry of propellant grains is uniform; however, variance in their geometry is present, and this has an impact on the performance of gun systems (Pocock, Locking, & Guyott, 2003). As a consequence, consideration needs to be given to the fact that propellant grains are variable in order to achieve improved accuracy during the IB simulation and burring rate calculation.

The actual gas delivery profiles resulting from real-life propellant differ from the propellant gas delivery profiles provided by simulation models. This study focused on determining the geometric variability of representative grain shape, namely Ball Powder. Assumption of geometric variability distributions were implemented to describe and simulate the geometric variability.

The initial goal of this study was to evaluate and characterise the effect of geometric variability among the grains on the combustion rates of propellants using both the closed vessel test and the dynamic firing test.

A second goal of the study was to define, formulate and implement Probability Distribution (PDF) functions into the relevant IB calculation tools, i.e. calculation of burning rate and simulation of the Internal Ballistic (IB) cycle of guns.

In summary, the identified samples that are characterised by their grain geometry show how they could influence the performance of the propellant, meaning that the IB simulation model results are affected by these phenomena. The results for both the tests and the simulation prove that the dimensions of the propellant grains are critical, even if the propellant samples have the same composition.

KEYWORDS: Internal Ballistic Simulation, probability distribution functions, propellant grains, closed vessel, dynamic firing test, ball powder, dynamic vivacity, geometric variability.

Table of Contents

LIST OF FIGURES

LIST OF TABLES

ABBREVIATIONS

STANAG	Standardisation Agreement
NATO	North Atlantic Treaty Organization
NWU	North-West University
RDM	Rheinmetall Denel Munition
MIC	Military Industries Corporation
PDF	Probability Distribution Functions
IB	Internal Ballistic
CV	Closed Vessel
SI	International System of Units
EPVAT	Electronic Pressure Velocity and Action Time

NOMENCLATURE

A_{burn}	Burning Surface Area
$A_{chamber}$	Chamber Area
A	Surface Area
a	Length of grain
B	Width of grain
C	Height of grain
^{o}C	Degrees Celsius
cc/g	Cubic centimetre/grams
D	Perforation diameter
dP/dt	Deferential pressure over deferential time
D	Web diameter
G	Grams
H	Height
j/g	Joules/gram
K	Degrees Kelvin
MV	Muzzle Velocity
MaxP	Maximum Pressure
MPa	Megapascal
ms	Millisecond
mm	Millimetre
P	Pressure
$\dot{r}$	Regression Rate
R	Burning Rate
S	Second
V	Volume
Z	Fraction

GLOSSARY OF TERMS

A Propellant Lot	Two or more propellant samples
A batch of propellant	Two or more propellant Lots
A form function	A function to calculate the volume and surface area of the propellant grains

GREEK AND OTHER SYMBOLS

β	Burn Rate Coefficient
n	Exponent Index
ρ	Density
f	Function
π	Pi
σ	Standard deviation
σ^2	Variance

CHAPTER 1: INTRODUCTION

1.1 Background

Propellant is an energetic material that burns extremely rapidly to produce heat energy and high-pressure gas, which are both used to accelerate a projectile forward. Propellant is also classified as a low-explosive material. This classification is relevant, since propellant burns perpendicular to the surface, layer by layer, and does not detonate. Propellant can also be classified as a polymer substance, thermoplastic material or smokeless gun propellant. The purpose of propellant is to create exceptional pressures within the chamber of a gun system. By means of gas generation, which happens when the grains start to burn and generate gases, both expansion and pressure propel the projectile forward (RDM Handbook, 2016).

There were several attempts by scientists to create a smokeless propellant for military purposes, the most successful of which was discovered by Paul Marie Eugène Vieille in 1884. This discovery led to the use of smokeless propellants in guns, which came to replace black powder. One of the primary advantages of smokeless gun propellant in comparison to black powder is that the generated pressure can be attained with less propellant mass, while the velocity of the projectile is increased up to 100 m/s (Tenney, 1943).

Over time, propellants evolved within military industries for numerous applications that varied from application in small arms ammunition, mortars, artillery projectiles, rockets, missiles and even the space shuttle for civilian industries. The many uses found for propellant prove its importance and versatility in a variety of applications.

There are various types of solid gun propellants that are used as gun charges based on their applications. These include:

- Single-base propellants (nitrocellulose, plasticiser and additives)
- Double-base propellants (nitrocellulose, nitroglycerin and additives)
- Triple-base propellant (nitrocellulose, nitroglycerin, nitroguanidine and additives)
- Nitramine-base propellant (cyclotrimethylene trinitramine RDX,

cyclotetramethylene tetranitramine HMX). Both of these have low flame temperatures, unlike the double-base propellants, which have the highest flame temperatures compared with all the above compositions (Agrawal, 2010).

Figure 1. 1: Various system configurations interfacing with propellants (Source: RDM Handbook, 2016)

Figure 1.1 demonstrates how the various propellant grain types are integrated into charges that are either contained in a conventional metal cartridge case (pictured left) or within a combustible case (pictured right) that burns away with the contents, adding to the propulsive effect (RDM Handbook, 2016).

1.2 Manufacturing of propellants

During the manufacturing process, the propellant can be softened by means of heating. The heating process then allows the propellant to be extruded into various shapes (RDM Handbook, 2016).

Solid gun propellants are homogeneous by nature (Agrawal, 2010). Propellants also contain a varying mixture of binder, plasticisers and solids. Each of the main types of these chemicals has its own unique manufacturing process and controlled parameters. The fact that certain constituents are manufactured from natural products (e.g. nitrocellulose) means that additional variables that are determined by conditions during their growing seasons can be introduced (RDM Handbook, 2016).

1.2.1 Ball powder propellant

In order to transform and shape the raw materials into a spherical double-base

propellant, a lacquer and aqueous solution must be mixed in a reactor. Figure 1.2 shows the production process of ball powder. The deterrent, solvent and stabiliser are added to the treated nitrocellulose in a lacquer along with a mixture of colloid and neutraliser (as an agent of an acidity reducer). During the two stages of adding the protective colloid, it will be agitated, and the base and the solvent will be separated from the non-solvent medium as an emulsion state. The process of heating the base and the solvent gradually into a distillate is done in the presence of a rotor to allow the granulation process to proceed, as shown in Figure 1.2. The product is single based but could be converted to a double-base propellant by impregnation (i.e. adding nitro-glycerine). The final product must then be dried and glazed (Botelho et al., 2015).

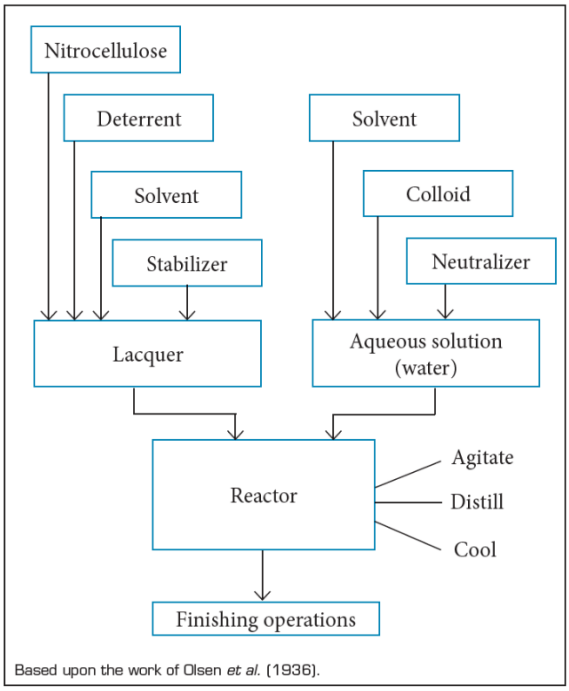

Figure 1. 2: Production process of ball powder (Source: Botelho et al., 2015)

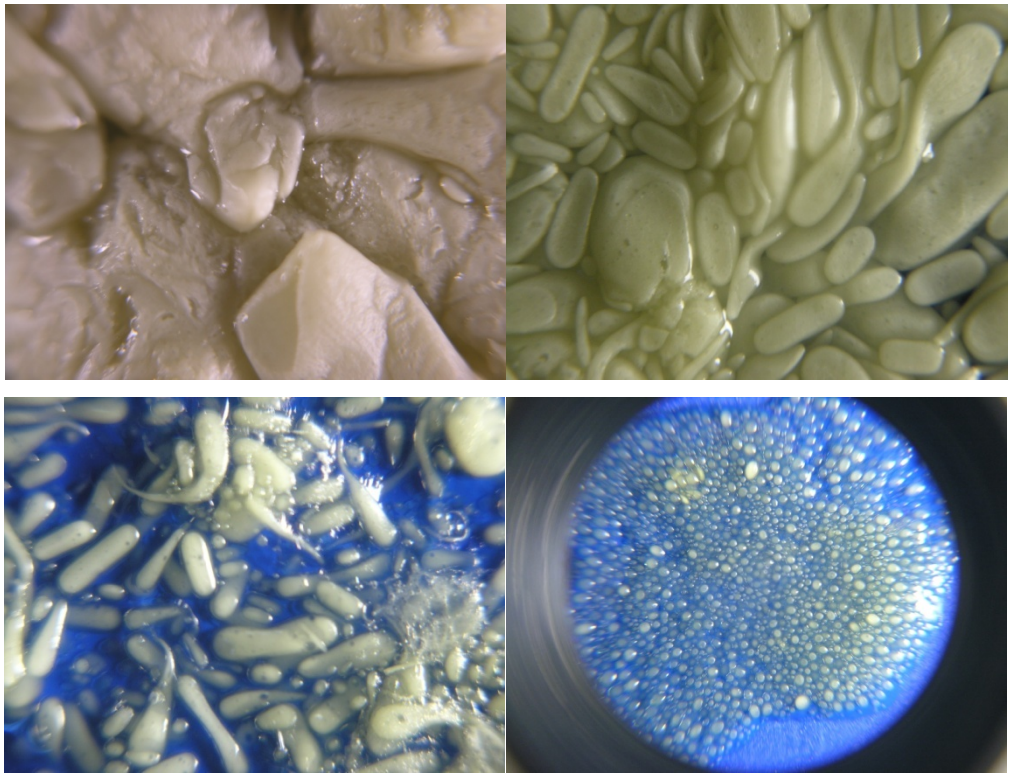

Figure 1. 3: Propellant manufacturing process: From top left: emulsion, semi emulsion; and then below left to below right shaping into a ball (Source: RDM Handbook, 2017).

1.2.2 Other shapes of propellants

Individual gun propellant grains are produced via a process of mixing raw materials, kneading or rolling them on heated rollers and then cutting them into flakes or extruding them for single or multiple perforations through one or more complex sets of dies. These could include some of the die pin designs that are indicated in Figure 1.4.

This process determines the internal configuration of the propellant and finalises it with the cutting process. By following the previous steps, but without using the die pin, the propellant will take the shape of a cord (RDM Handbook, 2017).

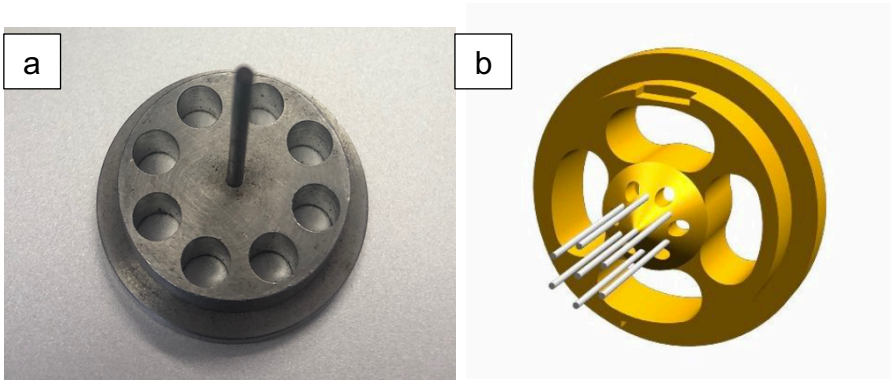

Figure 1. 4: Example of a die pin design for (a) single perforation and (b) seven perforations (Source: RDM Handbook, 2016)

1.2.3 General requirements for an ideal gun propellant

The following points summarise the essential attributes of a propellant suitable for use with ordnance propulsion elements, and which are usually required as a specification from end-users.

- It should not explode or detonate when subjected to suitable ignition;
- It should burn easily, producing hot gases at a low flame temperature (to preserve the barrel's life) as well as minimise muzzle flash and smoke (to prevent observation of the firing position);
- It should burn rapidly to generate gas that pushes the projectile forward within the barrel at high muzzle velocities;
- It should leave no residue in the barrel;
- It should be able to be processed into sheets, plates, rods and tubes for further processing into specific charge configurations;
- It should have sufficient mechanical properties (i.e. the grains should not crack when subjected to sudden pressure rises or acceleration within the gun barrel);
- It should have a long shelf life (RDM Handbook, 2017); and
- It should be able to be manufactured at a low cost (Bailey & Murray, 1989).

The above prominent features give the propellants unique characteristics that can be used to identify where they were manufactured, as well as their quality and safety.

1.2.4 Propellant burning rate and its geometry

When the propellant ignites the gas, a profile is built up during the time and temperature changes in the IB cycle. Thus, the burning rate (r) with unit (mm/s) is dependent on the (P) pressure, (β) coefficient and the (n) – which is the exponent index according to Vielle's Law (Kubota, 2002), as shown in the following equation:

$$\mathbf{r} = \beta \mathbf{P}^{n} \qquad \textbf{Equation 1}$$

In the methodology of the burning rate, the exponent is explained as a function of propellant formulation while the coefficient determined by the propellant starts burning (Agrawal, 2010).

The burning propellant surface recedes in layers that are perpendicular to the surface. In addition to the burning rate, the exact control of the various dimensional parameters ultimately determines the performance of the propellant and the conformance to the specification (STANAG 4367, 2000).

The burning rate is affected by the movement of grains in the chamber while the propellant is burning (STANAG 4367, 2000). Beside the variabilities of propellant grains geometric the movement of grains is illustrated as another factor that may influence the gas delivery profiles.

The propellant geometry and the linear rate of burning depend on the gas profile, which is defined by the chemical properties (Ball, 1960).

From Vieille's equation defined above, one can calculate the linear burning rate from closed vessel data of a specified propellant sample. Knowing the propellant grain geometry by measurement, one can calculate the pressure build-up in the closed vessel using the equation of state. By comparing the calculated pressure with the measured pressure, the burn distance as a function of time can be calculated iteratively (RDM Handbook, 2016). After taking the derivative of time and the log of the exponential, the n and β values can be calculated by linear regression.

$$\boldsymbol{d(t) = Iteration(P_{theor}, P_{meas}, t)} \qquad \textbf{Equation 2}$$

$$\boldsymbol{r(t) = \frac{d(d(t))}{dt}} \qquad \textbf{Equation 3}$$

$$\mathbf{\log r(t) = \log b + n \log P\ r(t)} \qquad \textbf{Equation 4}$$

Where:

P_{theor} : Theoretical pressure [MPa]
P_{meas} : Measured pressure [MPa]
$r(t)$: Burn rate [mm/s]
t : Time [s]

One of the purposes of this study was to investigate the propellant geometric variability of ball powder propellant and calculate the burning rate by applying Vieille's equation, as well as to research practical and appropriate methods to measure the geometric variability in terms of probability density functions as a standard output.

1.3 Key problem

Traditional gas delivery prediction calculation tools are based on exact form functions of a consistent and given geometric size, i.e. a function that calculates the burn surface and volume of the grain based on the geometry and burnt distance as input parameters – the so-called form function (RDM handbook, 2016). These form functions, which are used in IB simulation models, assume an exact homogeneous ballistic size and geometry of all the propellant grains in a charge during the burning of the grain layer by layer. The same assumption is also applied when performing burning rate calculations (STANAG 4367, 2000). This assumption is the ideal case and is not accurate in reality.

1.4 Problem statement

The traditional IB simulation model utilises a single average value (or set of values) that describes a propellant grain's geometry (RDM Handbook, 2016) and calculates the amount of gas generated by combustion, which is based on the geometry form function. A propellant charge contains thousands of propellant grains, and the existing method assumes all the grains have the same geometry. This assumption makes the IB simulation model less accurate. It also impacts the confidence between the IB simulation model and the actual dynamic firing tests.

1.5 Motivation

The proposed method used in this study should be able to improve the accuracy and predictive capability of IB simulation models for various propellant geometries. Furthermore, it would assist the ballistic system designers to define realistic and desirable propellant manufacturing specification tolerances in terms of propellant geometry.

1.6 Scope

The scope of the study was to investigate methods to characterise or measure propellant ball powder variability based on geometry. The results of the characterisation would then be used to develop a simulation code to evaluate the propellant's performance.

The research methodology could be applied to other grain shapes manufactured from solid gun propellant types used for gun charges, which were mentioned earlier in the background of the study.

The focus of the study is secondly on formulating and implementing methods to calculate propellant combustion gas delivery profiles based on geometric probability distributions. These formulations will then be implemented and tested in a Burn Rate Calculation algorithm as well as in a representative Internal Ballistic Simulation Model.

1.7 Project aims

The aim of the study was to improve the accuracy of IB simulation model codes by defining and implementing a proposed method that takes the geometric variability of propellant grains into account.

With the above discussion as a background, the aims of this study are to:

- Characterise the geometric variability of propellant grains resulting from the manufacturing process and develop probability distribution functions that describe this variability; and
- Define and implement general probability distribution form function functionality into the Burn Rate Calculation algorithm and the IB simulation model reflecting the influence of geometric variability on gas delivery profiles within the IB cycle.

1.8 Research objectives

The study will have the following objectives:

1. To investigate methods to characterise propellant grain geometric variability
2. To investigate methods to determine the distribution of the geometric variability of propellant grains by indirect measurement
3. To establish a baseline IB simulation model with the capability to simulate gas delivery profiles of geometric distributions based on the PDF functions.
4. To demonstrate the effects of propellant grain variability on ballistics in the weapon by a dynamic firing test
5. To demonstrate an improved IB simulation model from the traditional method of single average values to the new proposed method using PDF functions with included geometric variability.

1.9 Study limitations

This study focused only on the ball powder shape of the grain propellant. The objective was to develop and demonstrate the fundamental burning rate calculation and IB simulation. The research did not focus on multi-perforated, flake, or any other shapes of grain propellant.

1.10 Outline of the dissertation

Chapter 1: Introduction. This Chapter introduces the background of the study, defines propellants and explains their manufactured. The problem statement is also provided, as well as the scope, aim, objectives and contributions and limitations of the study.

Chapter 2: Literature review. This Chapter discusses previous studies regarding the geometry of propellant grains and the way they burn, as well as the calculations required for the form function of the various shapes of propellant grains and a description of the gases produced from the propellant burning.

Chapter 3: Methodology. This Chapter discusses the plans of subdivision and characterises and measures the ball powder propellant. In addition, this Chapter describes the procedure for the experimental work to test all the samples by a closed vessel test for maximum pressure (MaxP), differential pressure over differential time (dP/dt), and dynamic vivacity. In addition, all the samples will be tested by a dynamic firing test for pressure and muzzle velocity.

Chapter 4: Burning rate calculation and IB simulation models. This Chapter includes an explanation of both the IB simulation model and the burning rate calculation.

The proposed method and the traditional method were established in this Chapter for the IB simulation model and burning rate calculation.

Chapter 5: Results and discussion. This Chapter includes the results of the experimental work described in Chapter 4 and presents the simulation models.

Chapter 6: Conclusion. The final Chapter summarises the study, illustrates the findings and provides recommendations for future research avenues.

1.11 Summary

This Chapter introduced the propellant and the geometric variability of the grains as well as the factors that are affected by its performance during firing. The configurations of the various shapes of propellant and the ways in which they burn will be discussed in detail in the following Chapter.

CHAPTER 2: LITERATURE REVIEW

2.1 Introduction

In order to improve the efficiency of propellants, there are many properties that should be considered. One specific property is dimension size, which influences the gas delivery (Yildirim, 2012). Currently, IB modelling simulates the propellant size as uniform (STANAG 4115, 1997). However, in order to improve the current IB model, inclusion of the geometric variability of grains by means of the inclusion of a probability distribution is required. This will lead to more accurate IB simulation output in terms of pressure and muzzle velocity.

2.2 IB modelling

New chemical or physical properties of propellants can be simulated by means of computer models, as it provides an evaluation for the performance of the selected propellant within the shortest timeframe possible and with minimum cost (Horst & Nusca, 2006). Modelling enables the simulation of the effects of time without the constant need for experimentation, meaning that it can reveal previously unknown complexities (RDM Handbook, 2016).

In general, the simulation model can define system attitude and divergence into the model limitations. On the other hand, no simulation model code can provide results that are 100% accurate (RDM Handbook, 2016).

In order to predict the performance of a system, the necessary mathematical equations must be merged with a system simulation (Rousseau, 2013). In this study, the MATLAB software framework was used to implement the desirable codes for the relevant Internal Ballistic calculation algorithms and simulation models.

From chemical properties should identify the thermochemical properties (STANAG 4367, 2000) were gamma, specific energy (J/g), co-volume (cc/g), mass (Kg) and loading density (g/cc). These results were used as inputs for burning rate calculation and IB simulation. Flame temperature (k) was only used within IB simulation models.

Also included in all the models' thermochemical properties of ignition were specific energy (J/g), co-volume (cc/g) and mass (Kg) (STANAG 4400, 1993).

Co-volume and force are thermochemical parameters used to calculate the burning rate within the STANAG simulation model. With a known temperature, the force is described by STANAG 4115 as the released energy per unit of propellant mass.

The ideal gas law,

$$PV = nRT \qquad \textbf{Equation 5}$$

Where:

P: the pressure,
V: the volume,
n: the number of moles of the reaction gas,
T: the temperature in Kelvin and
R: the universal of gas constant = 0.0821 atm. L/mol. K (Poulsen, 2010).

Then the co-volume is stated in the Noble-Abel equation (STANAG 4115),

$$P\left(\frac{1}{\Delta} - \eta\right) = nRT \qquad \textbf{Equation 6}$$

Where:

P: Pressure (MPa),
V: Volume (cc/g),
Δ: Loading density (g/cc),
η: Co-volume (cc/g),
R: Universal gas constant = 8.314 (J/mol. K) and
T: Temperature (K)

the result of thermochemical properties that were used as inputs in burning rate and IB simulation model for this study, such as flame temperature (K), specific energy (J/g), gamma, co-volume (cc/g) and density (g/cc). All these units will be converted to an International System of Units (IS) using the simulation model according to STANAG 4115.

2.3 Surface area of propellants

With regard to explosive-filled propellants, changing the dimension of the grains is significant. Furthermore, the surface area of propellants plays an extremely important role in producing gas generation. The larger the surface area, the greater the gas delivery profiles produced with respect to confinement (Carlucci & Jacobson, 2008). This elaborates the influence of the propellant surface area on the gas delivery profiles.

The grain shape determines how consistently the propellant burns. However, just how rapidly it burns is ultimately determined by the geometry of the grain. The spherical shape burns over a very short distance. However, long, sustained burns require a web thickness of up to several metres for solid rocket propellants (RDM Handbook, 2016).

To study a propellant's behaviour, its physical dimensions need to be considered. By sieving the grains with various sieve sizes, as shown in Chapter 4, it was clear that there were size variations amongst the grains. This will affect the propellant's performance in terms of pressure and muzzle velocity.

2.4 Evolution of gases

In general, propellants contain nitrocellulose, which, when burnt, produces a sudden expansion of gases such as NO_2, N_2, O_2 and CO_2, as well as H_2O as steam at a high temperature and at a large volume (Bailey & Murray, 1989). The study by Bailey & Murray explains why propellants produce gases when changing their state from solid to gas in the presence of a sudden force.

When propellants burn in the presence of gas generated at high pressure, the chemical energy of the propellants will be converted into kinetic energy, causing projectile movement (Carlucci & Jacobson, 2008). The rate of gas evolution is therefore determined by the burning rate, the surface area and the density of the burning propellants.

The gas delivery rate (dm/dt) can be expressed by the following equation (Bailey & Murray, 1989):

$$\frac{dm}{dt} = r(t) * A * \rho$$ **Equation 7**

Where:

r: Linear burning rate [m/s]
A: Propellant grain surface area [m^2]
ρ: Propellant material density [kg/m^3]

2.5 Energy of propellants

Many factors and parameters change once the propellant is ignited. During propellant burning, energy is produced in the form of heat. The heat released by nitro-glycerine is calculated at 6,275 joules/gram (Bailey & Murray, 1989), and nitrocellulose is calculated as a heat release of 3,100–3,700 joules/gram. With the combination of the two compositions, the heat of the explosives will be within a range of 3,300–5,200 joules/gram (Agrawal, 2010).

Agrawal has explained the generation of gas delivery in a gun system as well as the mechanism of flame burning around the propellant grains over time. This energy takes the form of flames, which will roll along the grains. Each sequential layer ahead of the flame is preheated by the physical phenomenon and radiation, and the heat will therefore accelerate its decomposition until the ignition temperature is reached. Clearly, the higher the initial propellant temperature, the less heat will be needed to boost it to its ignition temperature, meaning that the rate of burning will be higher.

Although the impact of the charge temperature on the burning rate is small, it is still adequate to cause a considerable distinction in pressure and muzzle velocity that occurs in the weapon (Bailey & Murray, 1989).

2.6 Common propellant configuration used in gun propellants

Figure 2.1 shows that cord shapes, single perforation (or so-called tube) shapes and multi-perforation shapes, shown from top to bottom, respectively, affect the burning of the propellant as seen in Figure 2.2.

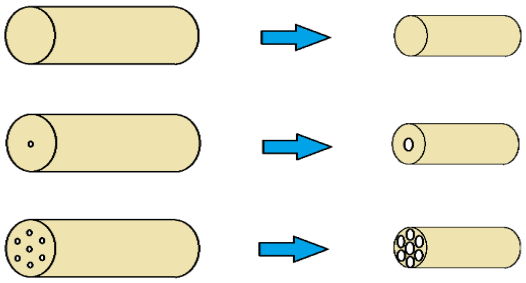

Figure 2. 1: Different propellant grain shapes (Source: RDM Handbook, 2016)

As shown in Figure 2.2, the shape of the propellant grains can be such that it can result in:

- Progressive burning, where the burning surface increases as the propellant is consumed (the multi-perforations shape shown in Figure 2.2);
- Neutral burning, where the burning surface remains constant as the propellant is consumed (the single perforation shape shown in Figure 2.2); and
- Digressive burning, or regressive burning, where the burning surface reduces as the propellant is consumed as a cord (the spherical shape shown in Figure 2.2) (RDM Handbook, 2016).

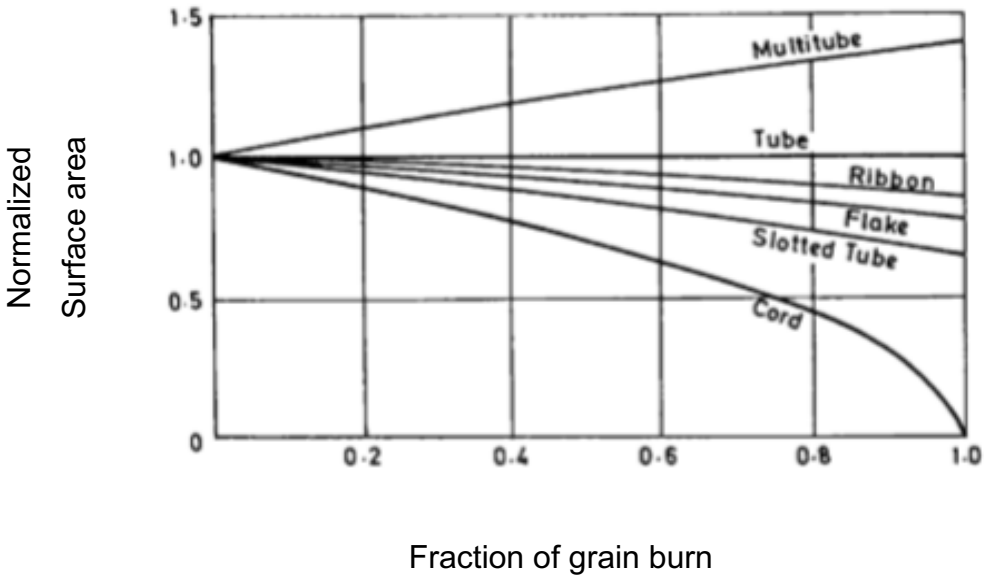

Figure 2. 2: Burning surface vs time curve for each shape, sequentially (Source: Bailey & Murray, 1989)

2.7 The burning and consumption rates of symmetrical and non-symmetrical propellant grains

For non-symmetrical single perforation propellants, the regression surfaces will break up prematurely, resulting in new and highly digressive moon-shaped surfaces early in the combustion cycle. This will affect the gas generation profile during the combustion cycle. The ideal geometry results in all propellant grains being consumed at the same instant, with maximum gas delivery over the full combustion cycle (Pocock, Neill, & Guyott, 2001).

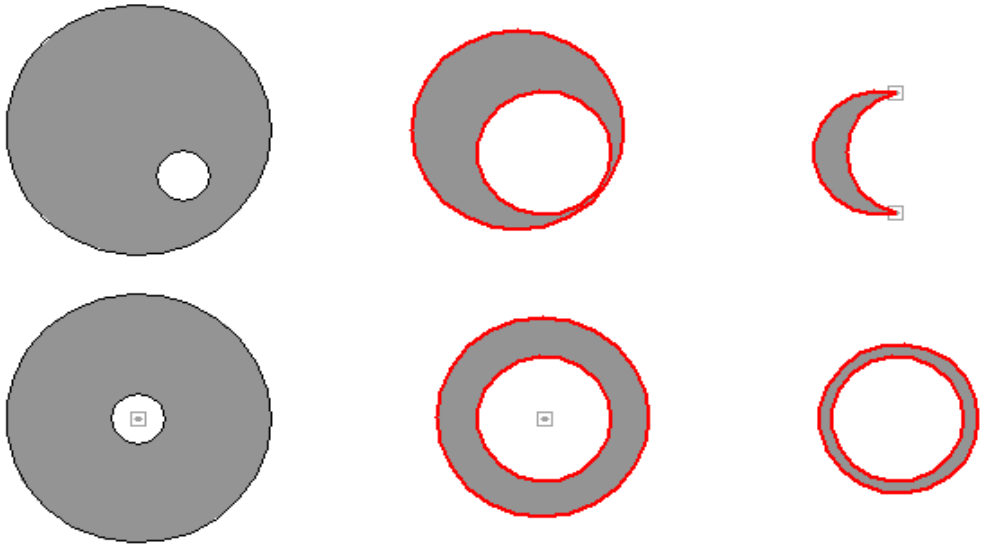

Figure 2. 3: Burning propellant for a single-perforation shape in symmetrical and non-symmetrical geometric (Source: Adapted from Pocock et al., 2001)

Pocock et al. (2001) noted that there was geometric variability among the grains, which they determined was because of the non-symmetrical extrusion phenomena.

For example, in single- and multiple-perforation grains, the perforation centre is not usually found in the middle of the grain due to geometrical variabilities. The diameter of the grains is also affected by these geometrical differences. Figure 2.3 illustrates the difference in burning between symmetrical and non-symmetrical geometries in single perforation grains.

The ball powder shape has geometric variabilities depending on the grain diameter, whereby the smaller grains are consumed before the larger grains. Although a ball powder shape was applied in this study, the possibility of using other propellant shapes would follow the same methods used in this study.

2.8 Grain dimensions

Within a single grain of propellant, the shortest straight distance between every two surfaces opposite to each other is known as a web thickness (RDM Handbook, 2017). A smaller web thickness means higher pressures, which result in a faster-moving projectile leading to an increased muzzle velocity, as shown in Figure 2.4. The optimisation of grain diameter and grain perforation diameter of the propellant increases the gas pressure and power, which enhances the muzzle velocity of the projectile itself. As a result, web thickness plays a critical role in improving the design of propellant grain (Yildirim, 2012).

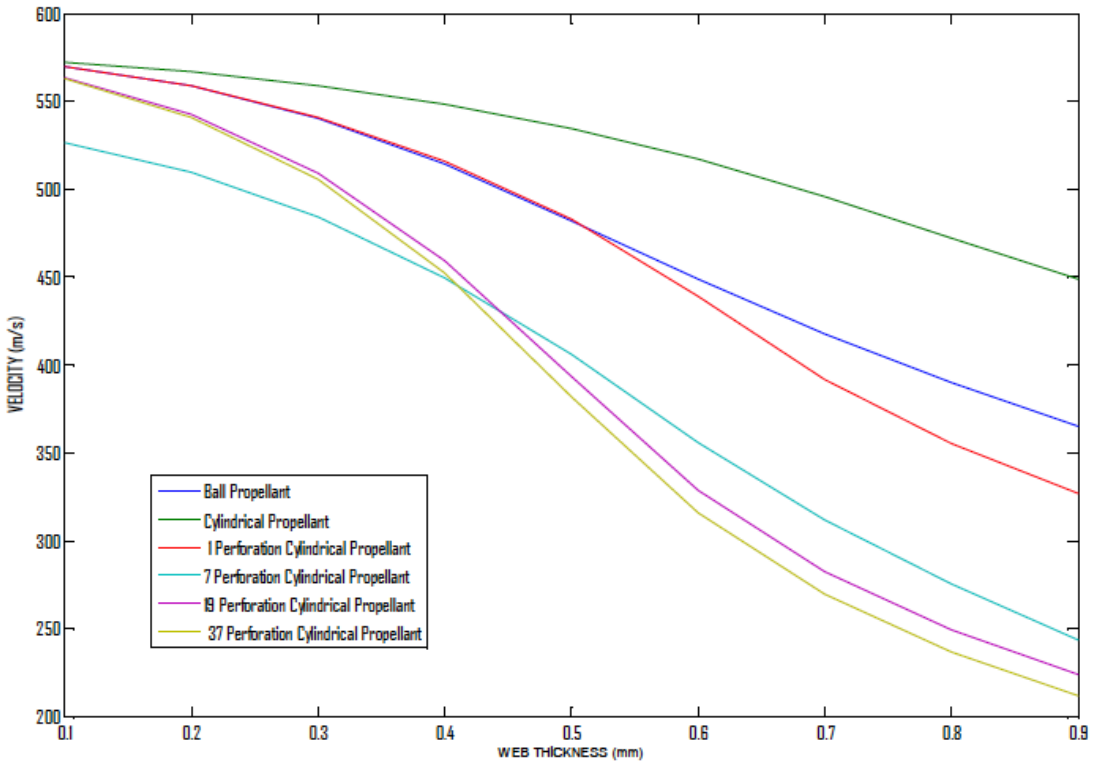

Figure 2. 4: Velocity vs web thickness curve for various shapes of propellant (Source: Yildirim, 2012)

The propellant will be completely used up when the last opposite burning side surfaces of the propellant grains have been consumed.

In the study by Yildirim (2012), the burning rate was determined by the optimum web thickness, which was obtained by studying the effect of the physical properties of the propellant grain. Both the grain diameter and the perforation diameter can greatly affect the web thickness, as a greater web thickness value produces less pressure and more muzzle velocity. This proves that web thickness plays an important role in propellant design. Furthermore, manipulating dimensions of propellant grains is easier than manipulating the chemical composition in order to achieve the best performance (Yildirim, 2012).

2.9 Probability distribution

If variability in the scientific data is presented, the use of statistical methods must be taken into consideration. In contrast, statistical analysis is unnecessary when the data are always the same (Walpole, 2012).

The probability distribution can be either discrete or continuous (Joyce, 2016).

In this study, the following types of probability distributions were used as input in the simulation model code, depending on the results of sample populations that had been obtained from the sieving process:

- Normal distribution
  The equation:

$$n(x;\mu,\sigma) = \frac{1}{\sqrt{2\pi\sigma}} e^{-\frac{1}{2\sigma^2}(x-\mu)\^2}$$ (Walpole, 2012). **Equation 8**

Where:

μ: is the mean
σ: is the standard deviation
σ^2: is the variance
x: sample
e: exponent

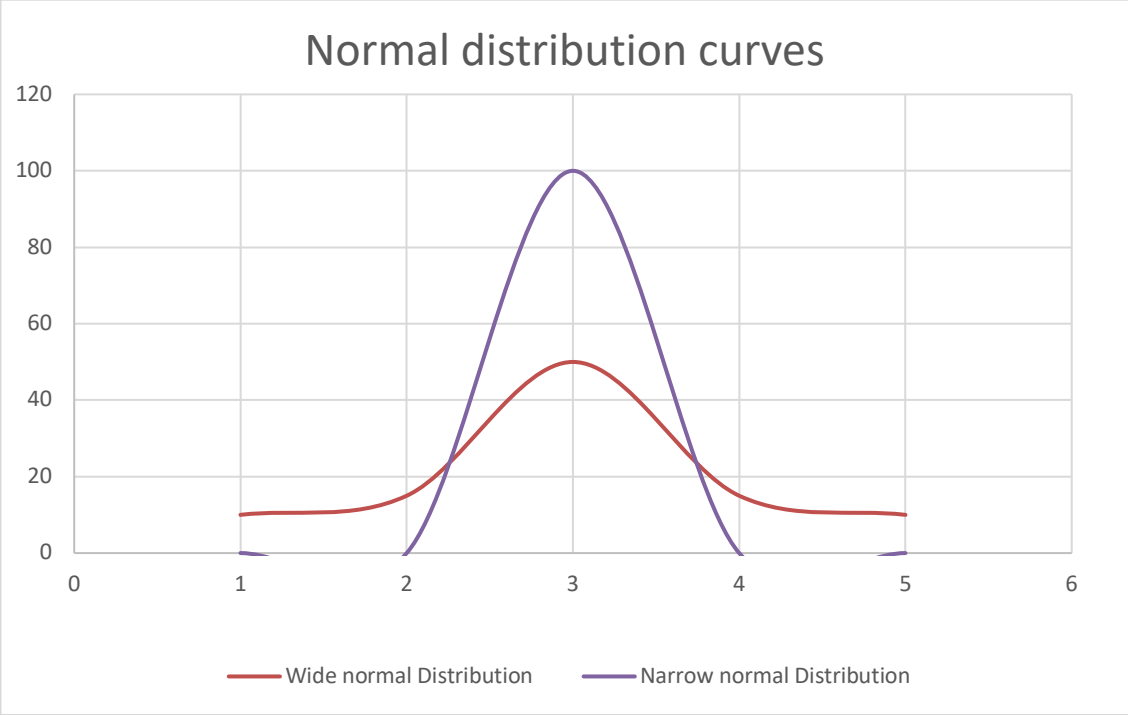

Figure 2. 5: Comparison of different normal curves (Source: Adapted from Walpole, 2012)

Normal distribution is commonly used in statistics to clarify a natural or artificial occurrence. In a normal distribution, the mean and standard deviation can cause differences in the distribution curve. Moreover, the normal distribution can be narrow or wide (bell-shaped). Therefore, it should be possible to compute the sample data by identifying the standard deviation and the mean (Walpole, 2012). Figure 2.5 shows that the wide curve contains the largest spread of size, while the narrow curve has the smallest spread in size.

- Gamma distribution

  The equation:

$$f(x;\mu,\beta) = \begin{cases} \frac{1}{\beta\,\alpha\,\Gamma(\alpha)}\, x^{\alpha-1}\, e^{-x-\beta} \\ 0, \end{cases}$$ **Equation 9**

Where:

α: Shape,
β: Rate (Walpole, 2012).

- Exponential distribution is a special gamma distribution when α equals one:

$$f(x;\beta) = \begin{cases} \frac{1}{\beta} e^{-x/\beta} \\ 0, \end{cases} \quad \textbf{Equation 10}$$

Depending on the density functions, normal, gamma or exponential can all be applied to studying different phenomena (Walpole, 2012).

In this study, the propellant samples were distributed in order to simplify the application of the simulation model depending on the results of sample populations that had been obtained by means of the sieving process to result in different size distributions. Distribution curves such as normal distribution (wide normal distribution), narrow normal distribution and gamma-skewed distribution were used.

2.10 Form functions

The volume or surface area of a propellant grain (or both) can be a significant parameter (measurement) for calculating the change in grain mass per millisecond in closed vessel tests. In general terms, when the grain starts to burn at all surfaces, whether naturally, digressively or progressively, mathematical equations should be applied to calculate the depth burned, using the volume and surface area of the grain (STANAG 4367, 2000).

In terms of simulating a new code, the volume and surface area of the propellant grains are required to calculate the function of the depth burned (STANAG 4367, 2008).

Table 2. 1: Form functions of popular shapes of propellants (ball propellant, flake propellant and single perforation) (Source: STANAG 4367, 2000).

Parameter	Ball Propellant	Slab Propellant	Single Perforation
Volume	$V = 1/6\ \pi\ D^3$ where V = volume r = radius of sphere D= grain diameter	V = a b c where V = volume a = length of grain b = width of grain c = height of grain	$V = 1/4\ \pi\ h\ (D^2 - d^2)$ where d = perf. diameter D = web diameter H = height
Surface Area	$A = \pi\ D^2$ where A = surface area	$A = 2\ (a\ b + a\ c + b\ c)$	$A = \pi\ [Dh+dh+D^2/2-d^2/2]$

This research has been undertaken to investigate how the variance in the surface area of ball powder propellant grain can affect a function of the depth burned.

The form functions represent the geometric variability in the surface area and grain volume, which are then used to simulate the combustion in an IB code for a ball powder propellant. In future research, it might be possible to adjust the form function to another appropriate shape of propellant, as shown in Table 2.1, but this is beyond the scope of work for this research, which only focuses on the ball powder.

In this study, the form function shown in Table 2.1 was used as a code written within MATLAB to represent the calculation of the surface area and volume for some shapes of propellant grains, as well as to derive the burning rate and interior ballistics based on the STANAG 4367 calculations.

2.11 Dynamic vivacity

Dynamic vivacity implies the amount of gas mass constant profile happening when the pressure starts to build up due to propellant burns. Two parameters can affect dynamic vivacity: physical properties and chemical combustion (RDM Handbook, 2017). One of the parameters used to accept propellant performance is dynamic vivacity. Dynamic vivacity is analysed by using the data obtained from closed vessel tests and could be used to evaluate the burning of grain surface area (Oberle, 2001).

$$DV = \frac{dP}{dt} \times \left(\frac{1}{P \times MaxP}\right) \quad \textbf{Equation 11}$$

Where:

DV: dynamic vivacity

P: pressure (STANAG 4115, 1997).

dP/dt is the derivative pressure over derivative time, which is the rate of the change in pressure over time (RDM Handbook, 2017).

MaxP is the maximum pressure recorded by a closed vessel test (RDM Handbook, 2017).

2.12 Closed vessel

The closed vessel is a suitable device for obtaining the vivacity and calculating the burning rate parameters (interior ballistics) of test samples (Baschung & Grüne, 2000).

Figure 2. 6: A closed vessel

The closed vessel is a closed chamber, available within RDM, which can have varying volumes, such as 105 cc, 300 cc and 700 cc, depending on the configuration of the propellant grains that need to be tested. However, in this study (for small arms ammunition), a volume of 105 cc was used. Each propellant sample is tested using a closed vessel by loading 20 g of propellant, sealing the vessel, and then firing it by igniting 1 g of black powder.

When propellant is tested inside the closed combustion vessel, the gas generated at high-pressure impacts with a piezoelectric sensor, which converts the measurement into a digital format (STANAG 4115, 1997). This pressure is then recorded by the RDM computer software.

According to the STANAG procedure to evaluate the propellant performance, a closed vessel test must be performed (STANAG AOP 7, 2003). The closed vessel shown in

Figure 2.6 was used during this study to test all the propellant samples and to record the gas profile created during the ignition and combustion sequence.

In a closed vessel, the solid propellant will convert immediately to gas that exerts pressure after ignition.

The parameter applicable in the closed vessel is the pressure trends over time to evaluate the propellant (Rodrigues et al., 2006).

In order to study gun performance, the burning rate of the propellants should be calculated. The force and co-volume obtained from the closed vessel must be ignored because of the errors that can occur as a result of vessel expansion and heat loss. On the other hand, parameters such as vivacity and quickness should be taken into consideration (STANAG, 4115, 1997).

2.13 Conclusions derived from previous studies

This Chapter explained the importance of geometry as well as what happens to propellants during and after burning. How the ballisticians applied the form functions on propellant diminutions was also discussed. The various types of propellant configurations were mentioned. After reviewing previous studies, this study used statistical analysis such as PDF and the sieving filtering method. In addition, the previous studies proved that the closed vessel is the best device to evaluate propellant samples in order to determine the vivacity, dP/dt and maximum pressure. The equation of burning rate provides a burning rate calculation to be incorporated with PDF. The evaluation of the propellant by experiments and simulation models will be discussed in the following Chapter.

CHAPTER 3: METHODOLOGY

3.1 Chapter overview

This Chapter provides details of the preparation and identifies the samples of propellant, as well as the methods of separating the propellant samples into sieves and then weighing them in preparation for the closed vessel and dynamic firing tests.

Two different batches of ball powder samples were utilised for the calibres, namely ball powder samples used in the 12.7 mm and 5.56 mm calibre weapons. All the samples were collected from RDM production plants, and the process is described in Figure 3.1. The samples were provided along with a full chemical analysis from the RDM laboratory.

This Chapter describes, in detail, the sieving process of disaggregating the grains into various diameter distributions. The weighing process necessary for the preparation of the samples is also discussed. The weighing process illustrates the fractions of the samples that have been taken from the sieve process, which will be used in all the tests described in this Chapter. After the weighing process, all the samples were prepared for the closed vessel and dynamic firing tests.

3.2 Introduction

The primary outcome of the proposed methods is to subdivide the propellant grain samples based on grain geometric variability to create different percentages from various grains, which change later from percentage to mass. Therefore, the 12.7 mm and 5.56 mm (ball powder) samples of propellants were gathered and characterised using a sieving process to separate and measure the different sizes of the grains.

All the propellant samples were stored in the propellant magazine under specific conditions (21˚C, 52% humidity).

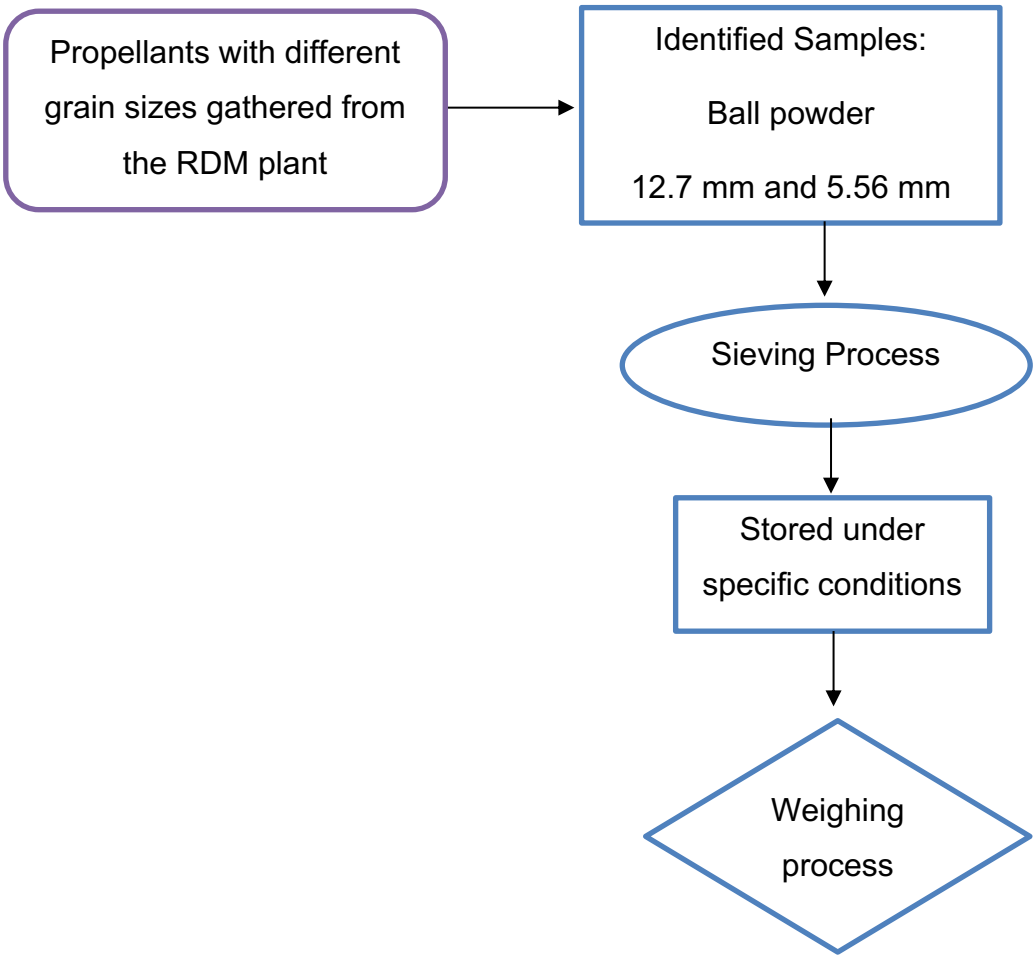

Figure 3. 1: Process flow diagram for sampling and evaluating process

Figure 3.1 shows the characterisation process of the different propellant samples utilised during this research. This involved performing the required measurements, such as the sieve process, which was conducted to separate and measure thousands of grains with different diameters.

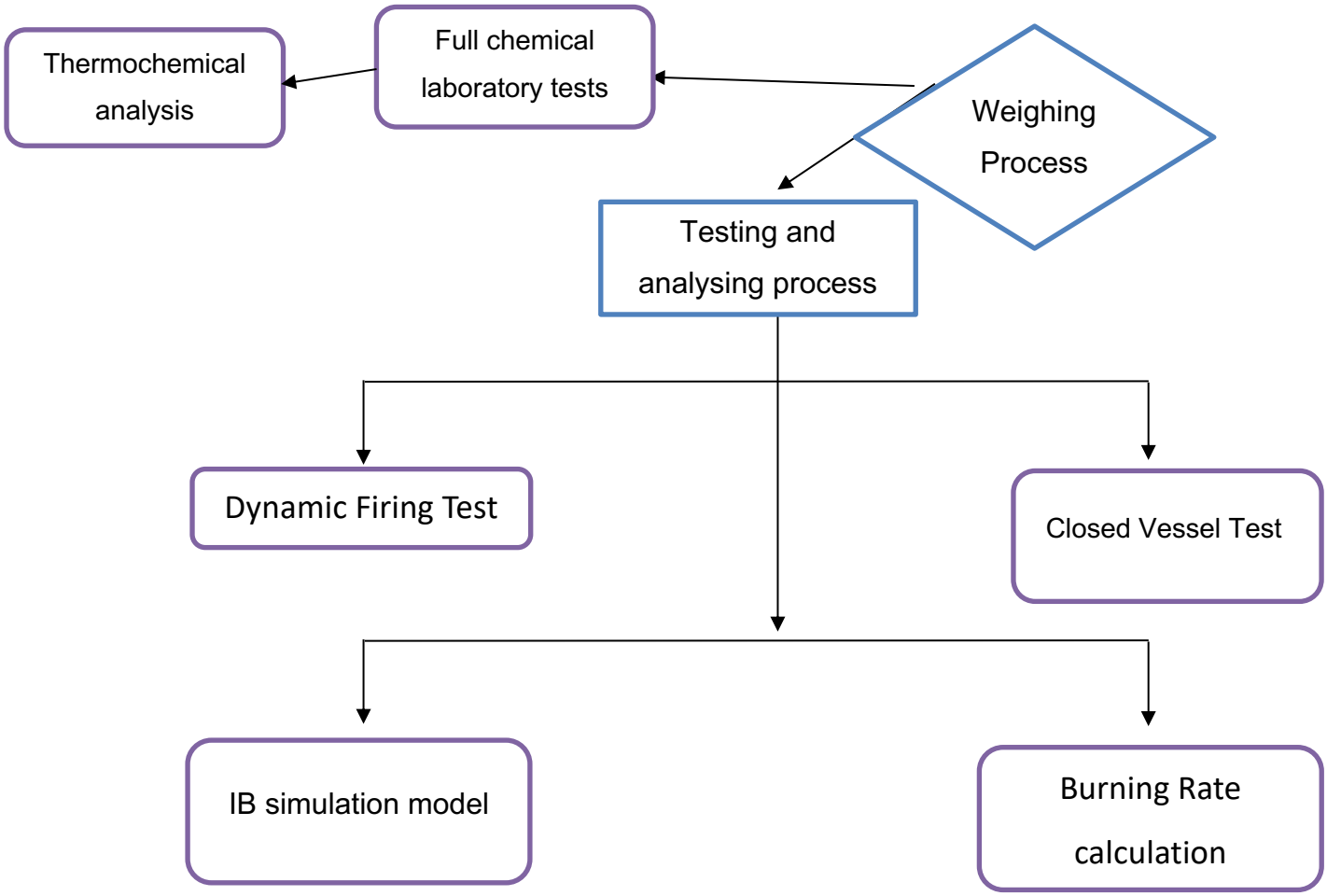

Figure 3. 2: Process flow diagram for testing and simulating propellant

Figure 3.2 shows the steps for testing and simulating propellant after preparing them with the weighing process.

In this study, two modules were used, as detailed in Chapter 4:

- The burning rate model for calculating the coefficient and index; and
- The IB model to calculate muzzle velocity and pressure.

3.3 Data collection techniques and instruments

Experimental data is essential for estimating parameters such as mean, standard deviation and variance (Walpole, 2012). In this section, data collection techniques will be used to identify the geometric variability phenomena in propellant grains as well as to generate scientific data.

Propellant samples from different production batches were selected for accurate measurement by means of manual and automated techniques, such as:

- The Wizcam device based on image processing, available for multi-perforated grains. This instrument has the capability to measure the web and holes by distinguishing between the light and dark (RDM Handbook, 2017). However, the device cannot measure small grains such as ball powder and flakes and can only measure individual grains. Therefore, it will not be used in this study.
- The sieve filtering method, which is a particle sizing and separation system for ball powders. This method is used to separate the particle sizes for ball powders and flakes by a range of sieves of increasing size. The advantages of this method are that it is a non-destructive test and that it has the ability to subdivide the different sizes of propellant grains to create probability distributions for the samples. However, it also takes a considerable amount of time to sieve the propellant grains and cannot measure the other propellant grain shapes. (Johannes, 2019).
- A moving bed micrometre, which is a particle sizing and characterising system to measure single perforation grains (Johannes, 2019). It can give accurate results and can measure all the dimensions of single-perforation grains, including the length and diameter, as well as the perforation diameter. However, it can only measure the grains individually.
- A dynamic light scattering spectrometer (Malvern). This instrument can measure the particle sizes for ball powders, flakes and single-perforation grains. It is accurate, rapid and easy to use (Rawle, Limited, Park, & Road, 2003). However, it is also a destructive test.

In this study, the sieve filtering method was only used for the ball powder propellant as it can measure particle size distribution and create representative samples.

3.4 Sieving analysis

Sieving analysis is an established process used widely in industry for research and quality control purposes. It is a cost-effective process, and a large number of grains

can be sieved this way. However, it takes time and is very labour-intensive (Rawle et al., 2003).

The sieving analysis is an indirect form of measurement, as it separates all the sample grains based on diameter tolerance. The samples are subdivided into groups (five groups are expected depending on the sieve analysis result), and then these groups are subdivided into subgroups by means of a weighing process to determine the appropriate distribution.

Therefore, this study has utilised a number of sieves with varying mesh sizes to obtain different distributions and to determine the fractions of the various grains within each size band/distribution band. The simplest way to evaluate the results is to arrange the samples in fraction groups. The sieving process helps control the size of the grains, thereby allowing determination of how the samples should be modified in order to be suitable for statistical analysis. Thus, sieves are used to separate the propellant grains according to their sizes and to create distributions. Table 3.1 shows the sizes of meshes in mm for the utilisation of the sieves.

Table 3. 1: Various sieve grid sizes

	Sieves opening (mm)	Sieves opening (mm)	Sieves opening (mm)
Small meshes	0.42	0.50	0.60
Large meshes	0.71	0.85	1.00

3.4.1 Objectives of sieving analysis

1. Measure the diameter of the grains in a micron (indirect measurement technique);
2. Define the variability among the grain sizes (i.e. the variability of the surface area of the grains);
3. Separate different grain sizes; and
4. Create grain size distributions.

3.4.2 The sieving process

The following steps form part of the sieving process in order to separate the different diameter size of the ball powder grains:

- Stack the sieves that have been chosen in Table 3.1 according to expected grain sizes.
- Gradually add the 12.7 mm propellant batch to the upper sieve.
- Shake the sieves until the smaller grains fall into the lower sieve.
- Shake the second sieve to allow the small grains to fall into the third sieve. The grains that did not fall through remain in the upper sieve along with the largest mesh.
- Repeat the process with the remaining sieves.
- Once all the sieves' surfaces are covered with grains, carefully transfer them to containers and clearly label the containers with the sieve size and batch number.
- Repeat the process with the rest of the batch.
- After the 12.7 mm propellant batch has been completed, repeat the same process for the 5.56 mm propellant batch.

After completing the steps shown above, different distributions were created by weighing different masses of two types of 12.7 mm propellants and 5.56 mm propellants from the containers, as indicated in the following section. All the samples were stored in the propellant magazine under specific conditions, and the closed vessel and dynamic firing tests were performed to analyse all the propellant samples.

3.5 The weighing process

After the sieving process comes the weighing process. This process begins with planning the percentages to make up the desired distribution and then converting these percentages to the masses needed for the closed vessel and firing dynamic tests.

The steps identified for the weighing process are:

1. Take out the ball powder propellant in each sieve and pour it into a container. Then, label and number the container according to the opening sieve size.
2. Bring all containers filled with propellant samples that have been sifted from the magazine to the weighing room.
3. Prepare the digital scales by cleaning and resetting them.
4. Open the first labelled container.
5. Put the labelled container on the scales and reset them. Weigh the required mass for each propellant sample in the labelled container according to the Tables shown in this Chapter.
6. Collect the data and prepare the samples for the closed vessel and dynamic firing tests.

3.6 The percentage of mass fractions for 12.7 mm and 5.56 mm samples

The distributions were not measured but rather determined and hard coded to see the effect later.

Tables 3.2 and 3.3 show how to subdivide the grains depending on the mesh sizes of the sieves to create propellant samples distributions. The percentage given to each sieve is considered a bin fraction. The next step after subdividing the percentage among the sieves was to use the percentages that were converted to mass in a unit of grams to fit with the appropriate propellant samples distributions.

In Tables 3.2 and 3.3, sample lot 1 is a normal distribution, and it is reasonable to expect some of the geometric variability may occur between the grains. Meanwhile, sample lot 2 is a narrow normal distribution, which takes into consideration whether the diameter of the grains was similar in size.

In Table 3.2, sample lot 3 is a skewed distribution that shows what would happen when most of the grain diameters had a greater size than the other samples.

Table 3. 2: The percentage of the fraction in various distributions for the 12.7 mm calibre

Distribution Samples	Sieve 1	Sieve 2	Sieve 3	Sieve 4	Sieve 5
	1.00 < 0.85 mm	0.85 < 0.71 mm	0.71 < 0.60 mm	0.60 < 0.50 mm	0.50 < 0. 42 mm
	Fraction (%)	Fraction (%)	Fraction (%)	Fraction (%)	Fraction (%)
Lot 1 – Normal distribution	10	15	50	15	10
Lot 2 – Narrow normal distribution	0	0	100	0	0
Lot 3 – Gamma-skewed distribution	35	25	20	15	5

Figure 3.3 shows an illustration chart for the grains size of the distributions for 12.7 mm. The chart shows the gamma-skewed distribution has the greatest percentage of large grains, while the narrow normal distribution has a grain size between 0.71 to 0.6 mm. Figure 3.3 shows that the probability distribution curve is the probability where the diameter size of grains would happen.

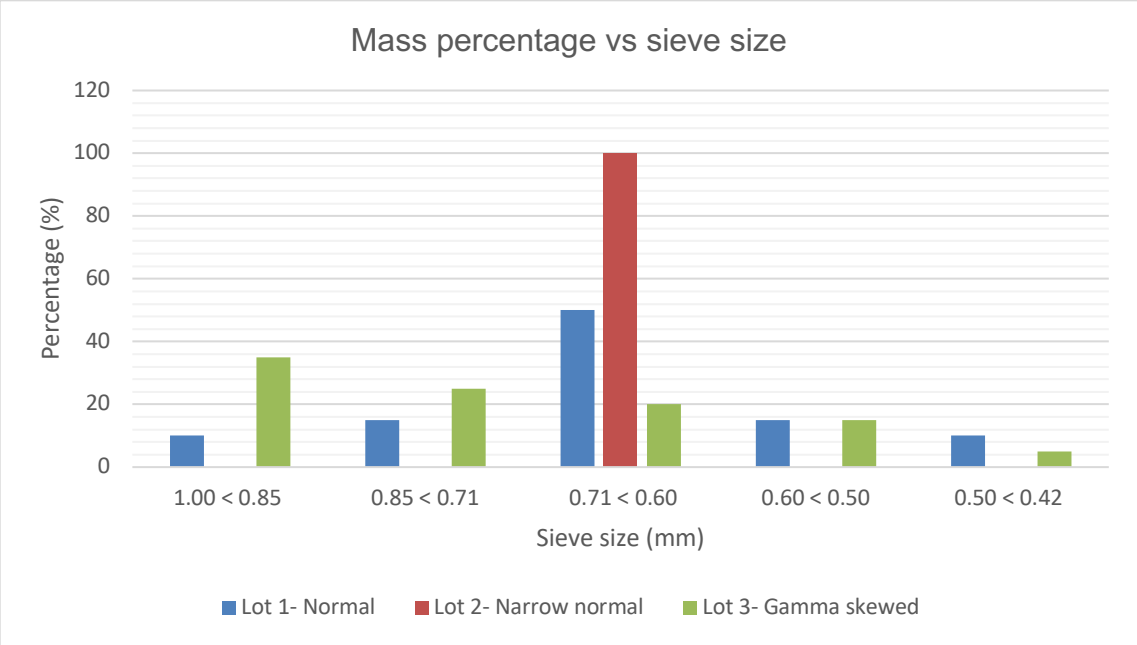

Figure 3. 3: The mass percentage of sieved samples to compose the various distributions for 12.7 mm

The sample lot 3 in Table 3.3 is a gamma-skewed distribution, which contains a high

percentage of grains with a small diameter size. Subdivided the samples determined by the grain size which available in the samples.

Table 3. 3: The percentage of fraction for various distributions for the 5.56 mm calibre.

Distribution Samples	Sieve 1 0.71 < 0.60 mm Fraction (%)	Sieve 2 0.60 < 0.50 mm Fraction (%)	Sieve 3 0.50 < 0.42 mm Fraction (%)	Sieve 4 0.42 < 0.30 mm Fraction (%)
Lot 1 – Normal distribution	12.5	37.5	37.5	12.5
Lot 2 – Narrow normal distribution	0	0	100	0
Lot 3 – Gamma-skewed distribution	10	20	30	40

Figure 3.4 shows the chart of a different fraction of the distribution for the 5.56 mm experiments. The chart shows the skewed distribution has the greatest mass of small grains, while the narrow distribution has a grain size of between 0.5 and 0.42 mm.

Figure 3.4 shows that the gamma-skewed distribution contains the largest amount of the smallest grain sizes.

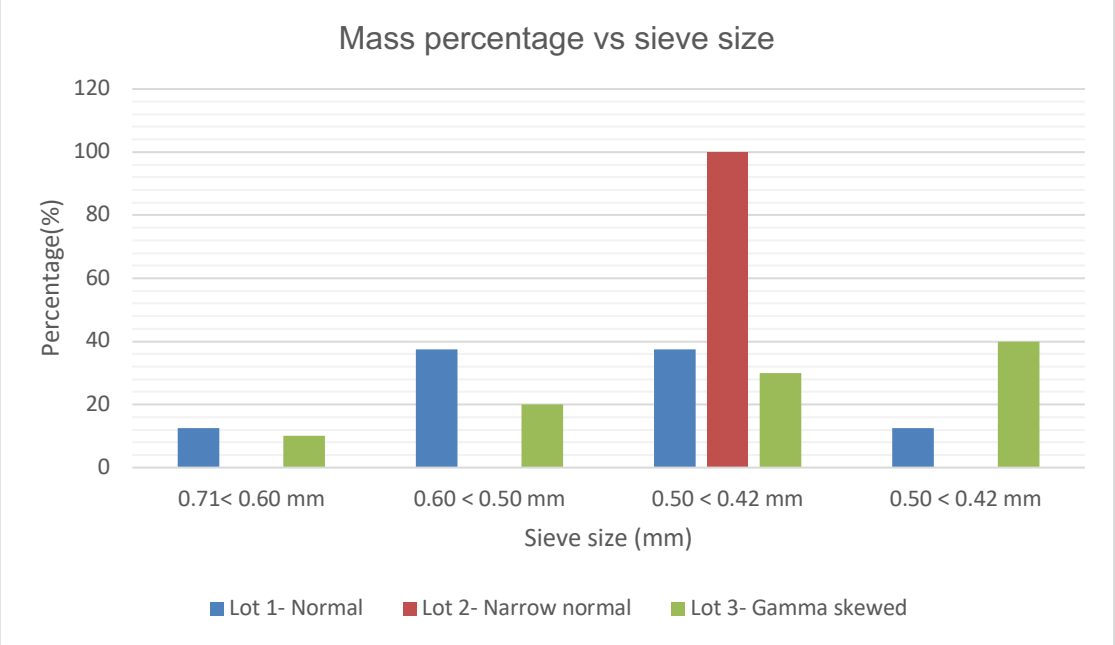

Figure 3. 4: The mass percentage of sieved samples to compose the various distributions for 5.56 mm

3.7 Fractions prepared and isolated for tests

From the specification of the samples, the actual size distribution (the diameter of grains) for 12.7 mm is 95% smaller than 1.0 mm, 90% between 1.0 mm to 0.50 mm and 3% smaller than 0.40 mm. The actual size distribution for 5.56 mm is 97% smaller than 0.71 mm, 90% between 0.71 mm to 0.40 mm and 3% smaller than 0.35 mm.

After the sieving process of propellant grains, the samples can be mixed in various combination fractions to yield a desired distribution. The number of distributions of propellant grains was limited by the sieves available. The percentages of the fractions in this Chapter are converted to mass. Figure 3.5 illustrates the geometric variability among the propellant grains for the 12.7 mm (A) and 5.56 mm (B) ball powders, respectively. These were separated by means of the sieving method.

A B

Figure 3. 5: Variability on the grains

The propellant mass is not the same in the closed vessel and the cartridge case in the dynamic firing test. For 12.7 mm and 5.56 mm, the required mass of propellant is 20 g for each sample. On the other hand, in the case of the 12.7 mm, the cartridge case is loaded with 16 g of ball powder; for the 5.56 mm, the cartridge case is loaded with 1.7 g of ball powder.

3.7.1 12.7 mm for the Closed Vessel test

The percentage was multiplied by the required mass for the test, as shown in Table 3.4, weighing and mixing the sample fractions to create different distributions. Twenty grams was the required total mass of each sample to be tested within a closed vessel. Each type of distribution needed three samples of 20 g. For each sample, three shots were prepared at the RDM test range. The samples were then fired in the closed vessel, and the average and standard deviations were calculated.

Table 3.4 shows how the 12.7 mm samples are subdivided into different distributions by weighing 20 g for each sample for the closed vessel test. The weighing process was repeated three times for each sample to obtain three shots.

Table 3.4 shows how to weigh the mass of each sample for the different distributions. The geometric variability between the grains was determined by the opening sieves, which is five sieves, as in the 12.7 mm calibre.

In comparison, the gamma-skewed distribution had the largest amount of large-diameter grains. On the other hand, in the narrow distribution, the grain diameter was between 0.71 and 0.6 mm.

Table 3. 4: The masses of the samples taken from the sieves for 12.7 mm

Distribution Samples	Sieve 1 Mass (g)	Sieve 2 Mass (g)	Sieve 3 Mass (g)	Sieve 4 Mass (g)	Sieve 5 Mass (g)
	1.00 > 0.85 mm	0.85 < 0.71 mm	0.71 < 0.60 mm	0.60 < 0.50 mm	0.50 < 0.42 mm
Lot 1 – Normal distribution	10%*20= 2	15%*20= 3	50%*20= 10	15%*20= 3	10%*20= 2
Lot 2 – Narrow distribution	0	0	100%*20= 20	0	0
Lot 3 – Gamma-skewed distribution	35%*20= 7	25%*20= 5	20%*20= 4	15%*20= 3	5%*20= 1

3.7.2 12.7 mm for the Dynamic Firing test

The method detailed in Section 3.6 was also applied, as seen in Table 3.5. The samples were subdivided into five different sieve sizes. From each sieve, a percentage

of mass was taken in order to fill the cartridge case with 16 g, which is the required mass for one shot. Three shots were needed in each sample.

Table 3. 5: Calculated mass taken from each sieve to create different distributions for 12.7 mm

Distribution Samples	Sieve 1 Mass (g)	Sieve 2 Mass (g)	Sieve 3 Mass (g)	Sieve 4 Mass (g)	Sieve 5 Mass (g)
Lot 1 – Normal distribution	10%*16=1.6	15%*16=2.4	50%*16= 8	15%*16=2.4	10%*16= 1.6
Lot 2 – Narrow distribution	0	0	100%*16=16	0	0
Lot 3 – Gamma-skewed distribution	35%*16= 5.6	25%*16= 4	20%*16= 3.2	15%*16= 2.4	5%*16= 0.8

3.7.3 5.56 mm for the Closed Vessel test

The geometric variability between the grains was determined by the opening sieves, which is four sieves, as in the 5.56 mm calibre. The required masses from the diameter sizes for the closed vessel test are listed in Table 3.6.

The methods from Section 3.6 were applied in Table 3.6. The percentages were converted to mass in order to create a different distribution for the closed vessel test. Each sample consists of 20 g.

Table 3. 6: The percentage of masses of the sample's series taken from the sieves for 5.56 mm

Distribution Samples	Sieve 1 0.71 > 0.60 mm Mass (g)	Sieve 2 0.60 < 0.50 mm Mass (g)	Sieve 3 0.50 < 0.42 mm Mass (g)	Sieve 4 0.42 < 0.30 mm Mass (g)
Lot 1 – Normal distribution	12.5%*20= 2.5	37.5%*20= 7.5	37.5%*20= 7.5	12.5%*20= 2.5
Lot 2 – Narrow distribution	0	0	100%*20= 20	0
Lot 3 – Gamma-skewed distribution	10%*20= 2	20%*20= 4	30%*20=6	40%*20= 8

3.7.4 5.56 mm for the Dynamic Firing test

As illustrated in Table 3.7, the samples were prepared for a dynamic firing test to investigate the effect of variability on the propellant grains. This was done by separating the samples into different distributions.

Table 3.7 shows the diameter size of the grains for the dynamic firing test. The required mass for one shot was 1.7 g. Three shots were needed for each sample, and the average was calculated from the three shots.

Table 3. 7: The different fractions of distributions for 5.56 mm and the required masses prepared for the firing test

Distribution Samples	Sieve 1 0.71 > 0.60 mm Mass (g)	Sieve 2 0.60 < 0.50 mm Mass (g)	Sieve 3 0.50 < 0.42 mm Mass (g)	Sieve 4 0.42 > 0.30 mm Mass (g)
Lot 1 – Normal distribution	12.5%*1.7= 0.2125	37.5%*1.7= 0.6375	37.5%*1.7= 0.6375	12.5%*1.7= 0.2125
Lot 2 – Narrow distribution	0	0	100%*1.7=1.7	0
Lot 3 – Gamma-skewed distribution	10%*1.7= 0.17	20%*1.7=0.34	30%*1.7= 0.51	40%*1.7= 0.68

3.8 Instruments used for the dynamic firing test

The following instruments were used in the gun to measure the required parameters for the dynamic firing test.

3.8.1 Piezoelectric sensor

A piezoelectric sensor was set up at the rear and/or at the middle of the gun chamber to measure the pressure. The piezoelectric pressure sensor, as shown in Figure 3.6, converts voltage to time in seconds and frequency to pressure in MPa (RDM Handbook, 2016).

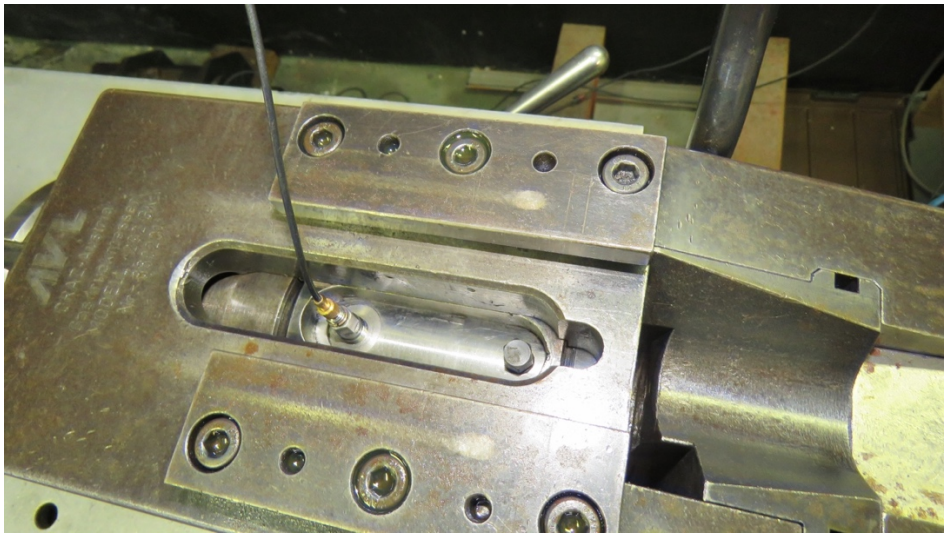

Figure 3. 6: The piezoelectric pressure sensor inserted into the chamber of the gun

3.8.2 Projectile Velocity Light Barrier

A projectile velocity light barrier was set up in front of the barrel, as seen in Figure 3.7, in order to measure how fast the projectile moves when exiting the muzzle of the gun barrel.

Figure 3. 7: A projectile velocity light barrier used to measure muzzle velocity

STANAG 4367 (2009) used four factors – the burning rate factor, the burning rate temperature factor, the force temperature and the down tube resistance – in order to adjust the IB simulation model to match the muzzle velocity and peak pressure obtained from the dynamic firing test during the influence of variation caused by the projectile mass and ambient temperature from shot to shot.

3.9 Conclusion

By means of the sieving and weighing processes, a different spread of samples will be applied in the form of distributions to test the ball powder samples in the different expectant geometric variabilities.

In this Chapter, the methodology described is applied. The prepared propellant samples distributions were fired by means of closed vessel and dynamic firing tests in order to verify and validate the IB model's obtained parameters, such as pressure and muzzle velocity.

Finally, all representative samples will be sent to the RDM laboratory for chemical analysis to identify the percentage of composition ingredients such as NC, NG, and Diphenylamine (DPA) detected by processes such as Gas Chromatography (GC) and High-Pressure Liquid Chromatography (HPLC), as seen in Appendix C. Then, the results that are provided by the RDM laboratory will be discussed in more detail in Chapter 4. All tests were conducted at the Rheinmetall Denel Munition Ballistic Proof Range.

Three propellant samples from each distribution were loaded into bullets – 16 g and 1.7 g for 12.7 mm and 5.56 mm bullets, respectively, as normally used for these calibres, as shown in Figure 3.8. The bullet was then loaded in the gun and fired, and the pressure and muzzle velocity were captured. In this study, the pressure in the dynamic firing test was used because it is more certain and can indicate how fast the

grains will burn, while the pressure in the closed vessel was used with time to calculate the dynamic vivacity.

Figure 3. 8: Cartridge case and projectile for 5.56 mm and 12.7 mm bullets respectively

The geometry of the ball powder shapes does vary, as shown in Figure 3.9, taken in RDM, which impacts on the simulated results of internal ballistics for propellants and reduced reliability.

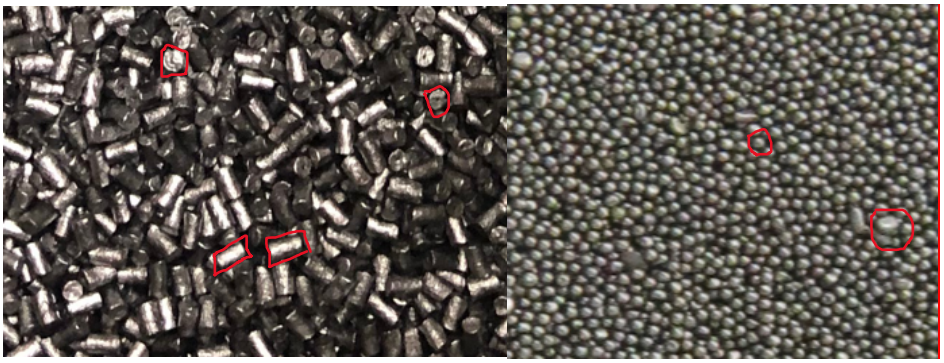

Figure 3.9: The geometric variability in single-perforation and ball powder shapes of propellant granules

3.10 Summary

In this Chapter, the batches of propellant were selected directly from RDM plants. Then, three of the propellant properties were used. First, the physical properties were

used to characterise and distribute all the samples by means of the sieving and weighing processes for ball powder propellant grains. Second, the chemical properties were analysed to determine the chemical ingredients and their percentages. Third, the thermochemical properties to use as required inputs for the IB simulation model.

This Chapter introduced the measurement used for the study, which is separated into two parts:

1. The sieving process, which is used to characterise the samples and to establish the average and standard deviation as well as the range of the propellant grains' diameter sizes. The specifications of propellant samples were provided with maximum and minimum grain diameter size. Moreover, this process is used to separate the different diameter grains of propellant samples in 12.7 mm and 5.56 mm for use in the weighing process.
2. The weighing process, which is used to prepare the propellant samples (12.7 mm and 5.56 mm) for the closed vessel and dynamic firing test. It also represents the probability of known geometric variability among the propellant grains.

Chapter 3 created real propellant distributions according to the available methods (i.e. sieves and mass fraction weighing). The practical measurement techniques described in this Chapter are used to prepare the samples for the closed vessel and dynamic firing tests. The research methodologies were applied to 12.7 mm and 5.56 mm ammunition propellant grains with geometric variability represented by propellant distributions samples created by the sieving and weighing processes. Propellant distributions samples were fired by closed vessel and dynamic firing tests.

CHAPTER 4: BURNING RATE CALCULATION AND IB SIMULATION MODELS

4.1 Introduction

All the samples were prepared in the previous Chapter for the closed vessel and dynamic firing tests. The following procedures for burning rate calculation and IB simulation model in this study are addressed below.

- Data sets were classified according to propellant type, geometric distribution type and application.
- Statistical analysis was performed to identify relevant PDF functions and related parameters.
- Input data was prepared for closed vessel and burn rate calculations based on the relevant requirements.
- Input data was prepared for an IB simulation model based on model code requirements.
  The output data of IB simulation model were processed in terms of relevant ballistic performance parameters.

In addition, this Chapter further details the outcomes of the closed vessel test, burning rate calculation and IB simulation model.

4.2 Outcomes of the closed vessel test, burning rate calculation and IB simulation model

Figure 4.1 illustrates the steps for the methodology, as follows:

1. Characterise each distribution's geometry based on average diameter value as well as appropriate theoretical derived distributions as measured or mixed with the sieves. Each data set distribution is accurately characterised as being as close to reality as possible. The single average value characterisation could clearly highlight the shortcomings of the traditional method.

2. Perform closed vessel tests for each sample type to obtain the raw pressure data (required for the burning rate calculation).
3. Calculate the burn rate based on the geometry assumption defined in the geometry characterisation. A set of burn rate parameters (coefficient and exponent) is always associated with a relevant geometry definition (whether single average value or PDF functions).
4. Perform dynamic firing tests of propellant samples distributions in the dynamic firing test and record all the results.
5. Finally, identify tendencies gained from the ballistic performance variations as a result of the various propellant sample distributions.

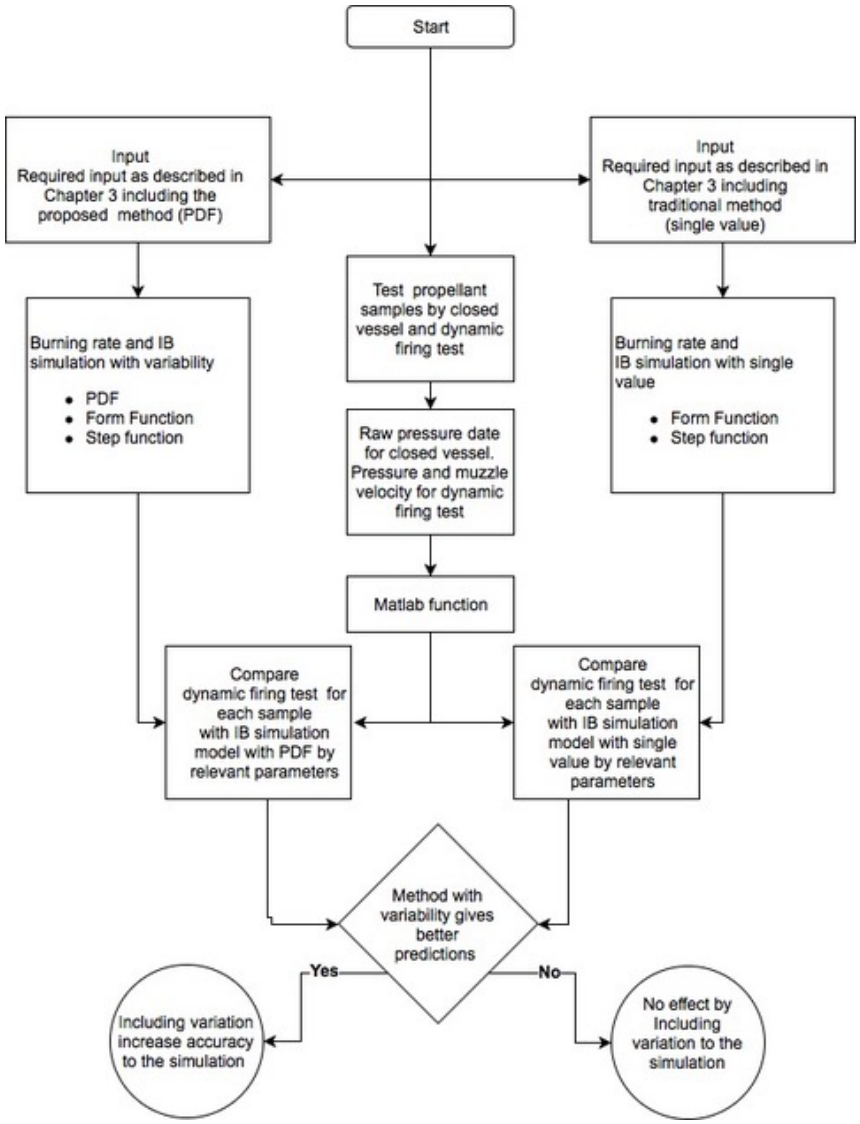

Figure 4. 1: Flow diagram showing the IB simulation models and all the tests

4.2.1 Outcomes of the closed vessel test

The results obtained from the closed vessel test are raw pressure data, which are used to calculate maximum pressure, dP/dt and the dynamic vivacity, as well as the raw pressure data used by MATLAB to calculate the burning rate.

4.2.2 Burning rate calculation layout

1. The results from the closed vessel test are imported (raw pressure data) in order to calculate the burning rate parameters (β) coefficient and the exponent index (^{n}).
2. A suitable MATLAB code with a single average value, as used in RDM to calculate the burning rate for all the samples, is identified.
3. Burning rate MATLAB code with PDF functions is implemented, which will consider the variability among the grains.

4.2.3 IB Simulation model layout

1. A suitable STANAG code is identified for IB simulation with the single average value method.
2. A proposed IB simulation model is implemented, which takes into consideration the variability among the grains by means of the PDF functions.
3. The results from the dynamic firing test (case mouth pressure and muzzle velocity) are compared with the IB simulation model results with single average value and PDF functions.

4.3 Formulation of gas generation simulation

This paragraph provides important background to the implementation and formulation of the gas generation calculation functions (i.e. the traditional single average value

method as well as the proposed method), to be utilized in the calculation of burn rate as well as in the IB simulation models.

4.3.1 Traditional single average value method

To calculate the theoretical gas delivery for the combustion of propellant composed of thousands of small grains of a given geometry type (spherical, tubular, cylindrical, etc.) in a propellant charge, it is assumed that all grains are of the exact same dimension, which is identified as the average grain dimension.

The form function calculations from Table 2.1 were used in the burning rate calculation and the IB simulation model for the ball powder to calculate the surface area and volume.

As described in Table 2.1, the volume of the ball powder grains is 1/6 π D^3; implemented in a form function as follows:

$$V_{grain} = \frac{1}{6}\pi(BS - 2d)^3 \qquad \textbf{Equation 12}$$

$$m_{grain} = V_{grain}\rho \qquad \textbf{Equation 13}$$

(RDM, Handbook, 2017).

Where:

m: mass [kg],
BS: Ballistic size,
ρ: propellant density [kg/m3],
V: the volume of the grain [m3].

The surface area and volume of individual grain were calculated by the following equations:

Initial condition:

$$(S_0,\ V_0) = Form(Type, BS, 0.0) \qquad \textbf{Equation 14}$$

During the ballistic cycle:

$$(S_i,\ V_i) = Form(Type, BS, d)$$ **Equation 15**

The gas fraction (the percentage of grains that burn) representing the form factor was calculated as follows:

$$Z\_i = 1 - \frac{V_i}{V_0}$$ **Equation 16**

Where:

V_i = volume after V_0,
V_0 = initial volume.

The initial burnt volume is zero. The burnt volume starts at zero and increases until it reaches 1, at which point the grain is consumed, meaning that the fraction will be 1. In other words, 100% of the grain is consumed, resulting in a total gas conversion.

$$M_{gas} = Z_i M_p$$ **Equation 17**

The Nobel-Abel State Equation was used in the IB simulation model to calculate the pressure during the ballistic cycle as seen in Appendix E:

$$P_i = \frac{M_{gas} F_p}{(V - \frac{(1-Z_i)M_{gas}}{\rho} - Z_i M_{gas}\eta)}$$ **Equation 18**

Where:

S:	Surface,
V:	Volume of combustion chamber,
Type:	Grain geometry,
d:	Burn distance,
i:	Index of time step,
Z:	Fraction burnt,
P:	Pressure,
M_p:	Propellant total Mass,
η:	Gas Co-Volume.

The gas fraction (Z), based on the form function, is the key to calculating the pressure in the chamber at any given time. The aggregate gas combusted can simply be calculated based on one individual grain geometry size, the total propellant mass and the density.

4.3.2 PDF functions method

Alternatively, the grain geometry sizes can be assumed to spread over some distribution of discrete values, designated as PDF functions, such as the typical normal distribution or a skewed distribution such as the gamma distribution, as seen in Figure 4.2. This is the more realistic assumption. The formulation to calculate the total gas combusted should now be based on the following equations:

Step 1:

Define the distribution of sizes based on propellant grain sizes measured:

As described in Section 2.9, for normal distribution, the following equation can be derived from equation 8:

$$PDF(x) = Normal(x|\mu, \sigma) \qquad \textbf{Equation 19}$$

As described in Section 2.9, for gamma distribution, the following equation can be derived from equation 9:

$$PDF(x) = Gamma(x|\mu, \sigma) \qquad \textbf{Equation 20}$$

Note that to ensure a general solution, the method should allow any relevant distribution function to be implemented. The above equations are implemented as discrete functions in the computer program with a set of discrete ballistic sizes against the probabilities:

$$\sum_{k=1}^{n} PDF(x_k) = 1 \qquad \textbf{Equation 21}$$

Where:

x: Ballistic size,
k: Index of discrete particle size,
μ: mean,
σ: Standard deviation.

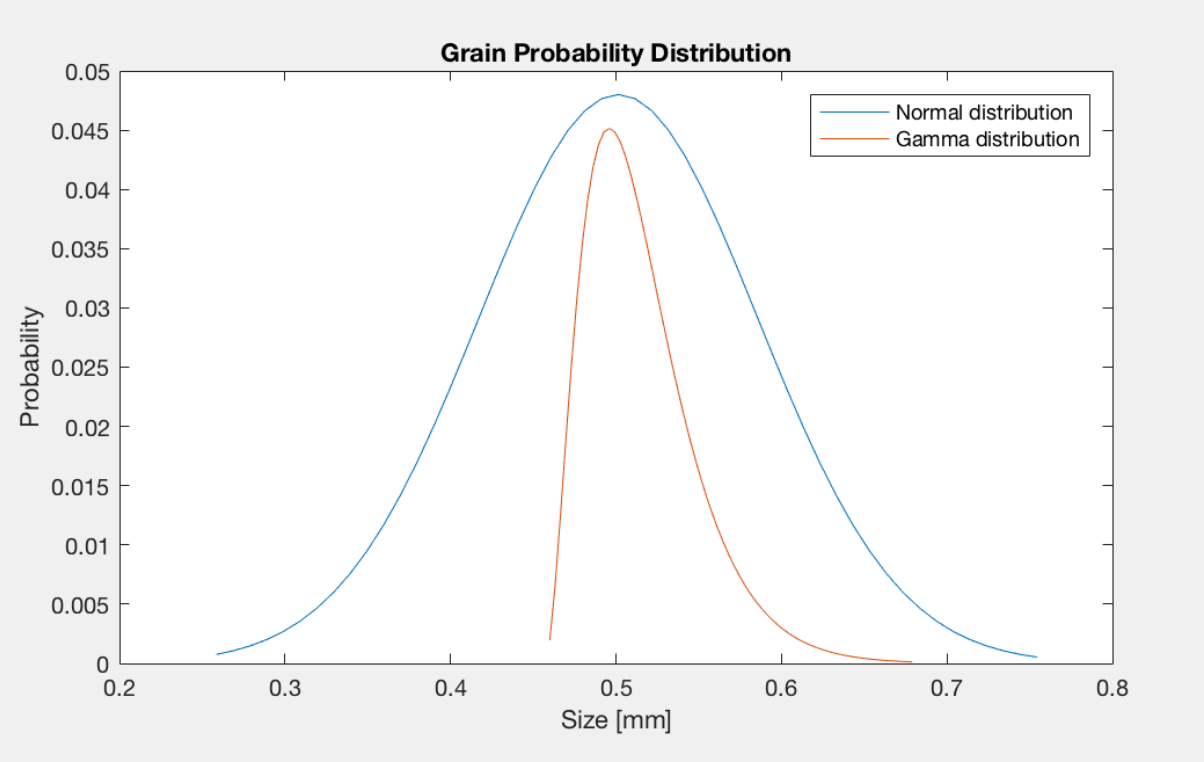

Figure 4. 2: Example Normal and Gamma Distributions of the same mean

Step 2:

Determine the initial mass and number of propellant grains at each discrete propellant geometry size. This is needed to calculate the total gas combusted at any given burnt distance. The principle was employed to base this calculation of propellant mass distribution:

$$M_k = PDF(x_k)\, M_p \qquad \textbf{Equation 22}$$

The number of grains per discrete size can then be calculated in order to determine the volume of the grains of each discrete size (which is needed to calculate the total gas combusted during the ballistic cycle):

$$n_k = \frac{M_k}{V_{k0}\, \rho} \qquad \textbf{Equation 23}$$

Where the initial surface and volume for each discrete ballistic size in the distribution is:

$$(S_{k0}, V_{k0}) = Form(Type, x_k, 0.0)$$ **Equation 24**

Before combustion starts, the Aggregate (total) Initial Grain Volume equals:

$$V_0 = \sum_{k=1}^{n} V_k$$ **Equation 25**

Verification check:

$\sum_{k=1}^{n} M_k$ should be exactly M_p **Equation 26**

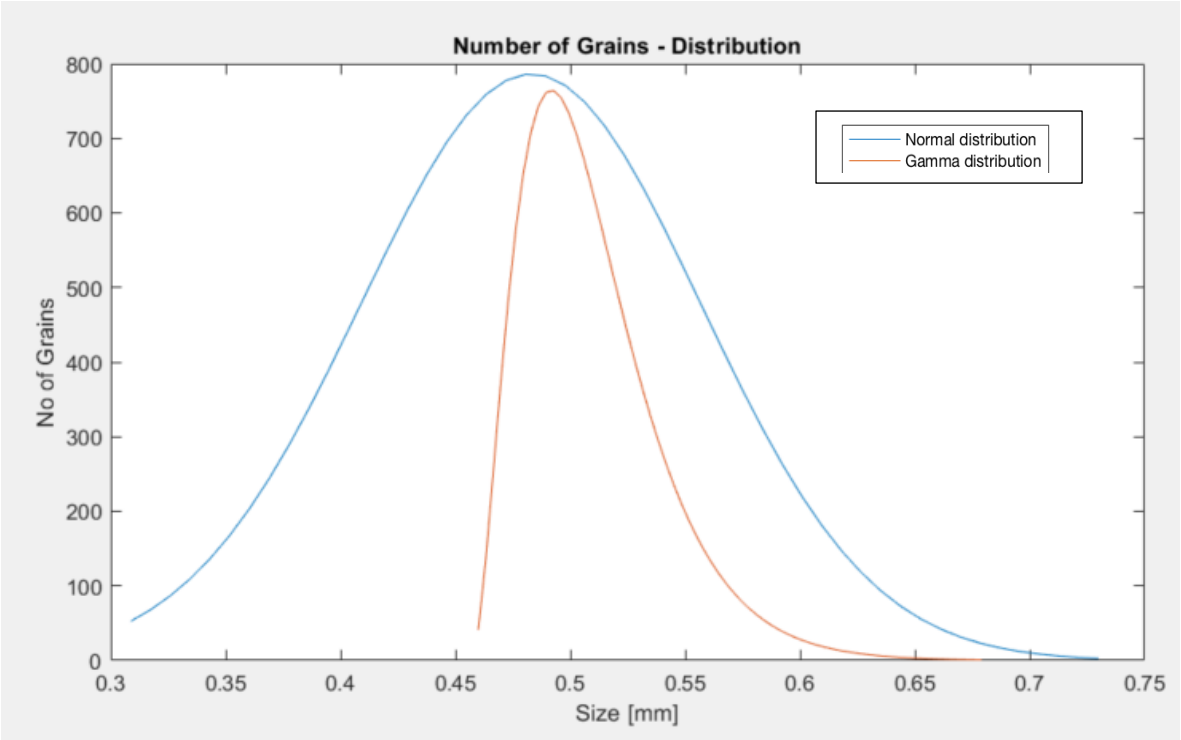

Figure 4. 3: Example of the number of propellant grains as a function of ballistic size for two distributions of the same mean

The initial condition for the ballistic cycle has been defined by the first two steps. The next step is then employed in the ballistic cycle to calculate the propellant mass combusted and the pressure during each time step.

Initial Gas Fraction is obviously 0:

$$Z(0) = 1 - \frac{V(0)}{V_0} = 0, since\ V(0) - V_0$$ **Equation 27**

Step 3:

The propellant gas mass can be calculated during the ballistic cycle based on the following equations:

$$V(i) = \sum_{k=1}^{n} n_k \, Form(Type, x_k, d) \qquad \textbf{Equation 28}$$

And:

$$Z(i) = 1 - \frac{V(i)}{V_0} \qquad \textbf{Equation 29}$$

Now that total gas fraction is known, equation 29, as defined above, can be employed to calculate the total gas mass combusted.

$$Mgas(i) = Z(i)M_p \qquad \textbf{Equation 30}$$

Now, the subsequent calculation cycle is exactly the same as for the single average value method described in Section 4.3.1. The smaller propellant grains will vanish first and the bigger grains progressively as the burn distance increases, exactly accounting for the distribution of grains in the propellant charge in the dynamic firing test.

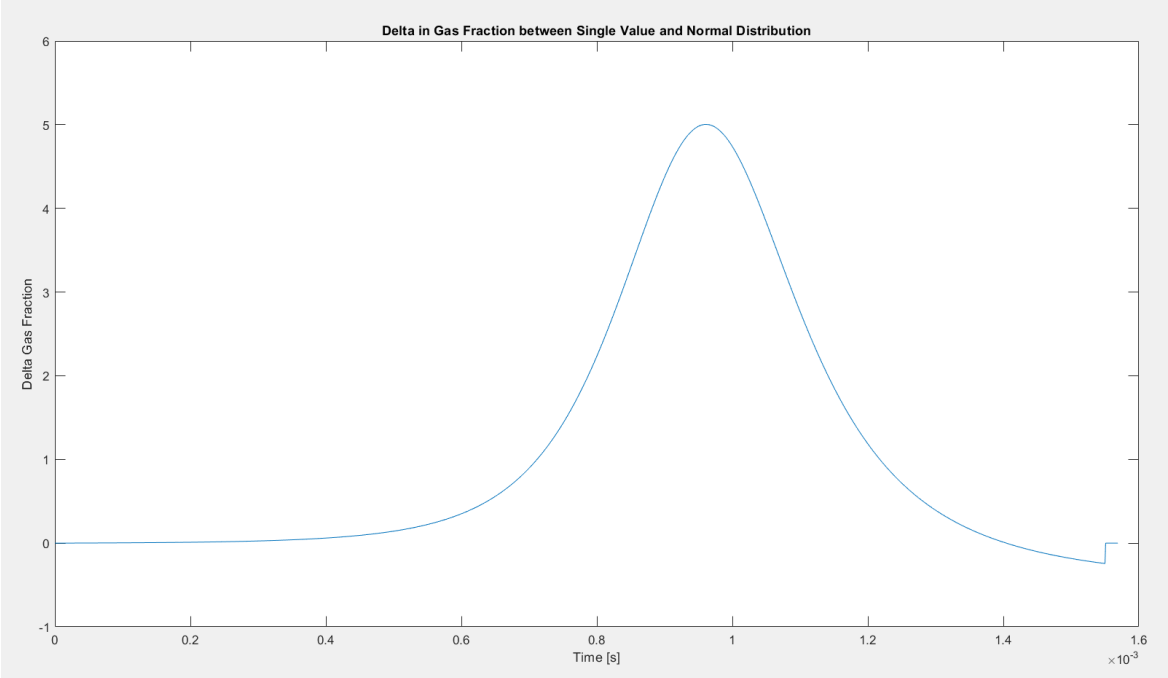

Figure 4. 4: Delta in gas fraction between single average value and normal distribution

Figure 4.4 shows an example illustration of the difference in gas fraction versus time in the simulated ballistic cycle between the single average value method and the PDF function for the normal distribution of the same mean value.

The proposed improved method uses the same form function calculation for an individual grain, but the geometry of the propellant grains is defined over a discrete distribution of values, thereby representing the charge composition of the propellant grains more realistically. For example, the average diameter of a ball propellant charge is 0.81 mm. In the traditional method, this size is assigned to all the propellant grains in the charge, and the form function gas delivery calculation is based on this size. With the new proposed method, this size will vary from a small to a large value based on the type of distribution of the grain sizes in the charge. The calculation of gas delivery will then be based on this size distribution (i.e. the smaller grains will be consumed before the larger grains).

4.4 Required inputs for an IB simulation model

In addition to the configuration and mass of the propellant, the specifications of the weapon, such as chamber volume [cc], barrel groove length [mm], calibre [mm] and projectile mass [g], were also included as seen in Appendix E.

4.4.1 Geometric variability distributions

Table 4.1 and 4.2 show how to generate the diameter size of the grains in the burning rate calculation and IB simulation model for 12.7 mm and 5.56 mm. These generated data were theoretical assumptions to the geometric variability on the propellant grains and were designed to illustrate the influence of the proposed method in comparison to the single average value method.

As described in Table 4.1 for 12.7 mm, the grains in each distribution were varied from the maximum to the minimum, with the average grain diameter assumed to be 0.7 mm. But with the single average value, the diameter of every grain was 0.7 mm. Obviously, the standard deviation for a single average value is zero because all the

grains are exactly the same size. The standard deviation of the very narrow distribution was the smallest, followed by the narrow distribution. The average grain diameter in all the distributions in both methods is the same as the single value grain size in order to illustrate the influence of various distributions against the single average value method.

Table 4.1: Geometric grains 12.7 mm for different samples

Geometric distribution	Average Diameter	Maximum Diameter	Minimum Diameter	Standard deviation
Normal distribution	0.7	0.92	0.50	0.116
Narrow normal distribution	0.7	0.71	0.60	0.042
Very narrow normal distribution	0.7	0.69	0.65	0.019
Gamma skewed distribution	0.7	0.92	0.50	0.148

As described in Table 4.2, for 5.56 mm, the grains in each distribution were varied from the maximum to the minimum, with the average grain diameter assumed to be 0.5 mm. But with the single average value, the diameter of every grain was 0.5 mm. Obviously, the standard deviation for a single average value is zero because all the grains are exactly the same size. The standard deviation of the very narrow distribution was the smallest, followed by the narrow distribution. It is important that the average grain diameter in all the distributions in both methods is the same to ensure a one-to-one comparison in the simulation results (i.e. the influence on ballistics of grain distribution alone is isolated).

Table 4.2: Geometric grains 5.56 mm for different samples

Geometric distribution	Average Diameter	Maximum Diameter	Minimum Diameter	Standard Deviation
Normal distribution	0.5	0.66	0.43	0.071
Narrow normal distribution	0.5	0.55	0.48	0.037
Very narrow normal distribution	0.5	0.52	0.50	0.010
Gamma skewed distribution	0.5	0.61	0.48	0.038

4.4.2 Required inputs

Within the burning rate calculation, which calculated the total number of grains, the following equation was applied:

$$\text{Number of grains} = \frac{\text{m}}{\text{V}*\rho} \quad \textbf{Equation 31}$$

The Nobel-Abel equation is required in the IB simulation model to calculate theoretical pressures:

$$P\ (V - mg\ b) = Mg\ RT \quad \textbf{Equation 32}$$

where:

P: the pressure, V: the volume of the gas created, Mg: the mass of the gas, b: the co-volume, T: the temperature in Kelvin and R: the Universal Gas constant = 8.314 (J/mol. K)

This equation could apply in the volume of ball powder grain, as seen in Table 2.1.

$$V = 1/6\ \pi\ D^3 \quad \textbf{Equation 33}$$

The volume during any time

$$V(t) = 1/6\ \pi\ [d(t)]^3 \quad \textbf{Equation 34}$$

This equation allows us to calculate the mass of gas over time:

$$Mg(t) = \rho\,[\,V0 - V\,(t)] = \rho 1/6\,\pi\,[D3 - [d(t)]\,3 \quad \textbf{Equation 35}$$

According to the conservation of mass, mass can neither be created nor destroyed. Thus, the amount of propellant burnt, and the amount of gas created are equivalent.

In the weapon, the mass of the gas profile according to the gas law can be given as follows:

$$PV = Mg\ RT\ or\ P = \rho RT \quad \textbf{Equation 36}$$

(Carlucci, 2007).

The following equation calculates the gas thermal energy for the IB simulation model:

$$E\ gas\ =\ C\ gas\ C\ v\ T\ gas \qquad \textbf{Equation 37}$$

where:

C_{gas}: Gas mass combusted,
C_{v}: Heat capacity at constant volume and
T_{gas}: Flame temperature (RDM, Handbook, 2017).

4.4.3 Chemical and Thermo-Chemical properties

In this study, representative propellant samples were sent to the RDM laboratory for analysis. The results from these tests, as seen in the Appendix C, were used to calculate the thermochemical composition (using a program from Fraunhofer Institute for Chemical Technology, or ICT), as shown in Table 4.3. The thermochemical properties must be inserted via a MATLAB code to construct burning rate and IB simulation models.

Table 4.3: Thermochemical parameter values

Propellant	Thermochemical parameters	Value	Unit
5.56 mm (ball powder)	Pressure	258	MPa
	Specific Energy	1028.3	J/g
	Gamma	1.2417	
	Density	1.592	g/cc
	Co-Volume	1.016	cc/g
	Flame temperature	2980	K
12.7 mm (ball powder)	Pressure	236	MPa
	Specific Energy	934.3	J/g
	Gamma	1.2584	
	Density	1.569	g/cc
	Co-Volume	1.048	cc/g
	Flame temperature	2586.1	K

4.5 Summary

In this Chapter, PDF functions were represented by normal distribution and gamma-skewed distribution equations to calculate the gas delivery profiles against single average values. PDF functions and single average value were incorporated within the IB simulation model and burning rate calculation.

Geometric variability distributions were represented by generate assumed propellant grains diameter depends the on sieving and weighing process. Geometric variability distributions and single average values were imported to the IB simulation model and burning rate calculation.

The following Chapter will focus on the results obtained from the closed vessel and dynamic firing tests as well as the outputs obtained from the burning rate calculation and IB simulation models. In addition, the next Chapter will determine whether we can detect the same tendencies with simulations using the traditional geometry approach together with the new approach of distribution functions in line with the objectives of the study. If the new approach simulations show improved correlation with the experimental observations over the traditional method of single average values, it will lead to an improvement in the simulation capability.

CHAPTER 5: RESULTS AND DISCUSSION

5.1 Introduction

In this Chapter, the results of the closed vessel test, the dynamic firing test, the burning rate calculation and the IB simulation model are discussed. In addition, a comparison is made between the IB simulation model with the proposed method and the IB simulation model with the traditional method (single average value), which assumes all the propellant grains are the same size and uses a single average diameter size for all grains. The results of these models are then compared against the dynamic firing results.

The representative grain diameter was generated under the assumption that the variability between the propellant grains followed a normal distribution and gamma-skewed distribution, with the same mean but different variances. The data was then used to calculate the burning rate. The IB simulation model theoretically simulates the propellant distribution samples. So, one single average value simulation was compared against the various PDF's for each calibre. This would illustrate the capability to evaluate propellant distribution with the proposed method, whereas with the traditional single value method it is impossible.

The discussion has three parts. First, the effect of geometric variability on propellant performance for the propellant distribution samples in closed vessel and dynamic firing tests is discussed. Second, the outputs of the burning rate calculation, obtained with the proposed method and with single average value as used in RDM, are compared. Third, the output of the IB simulation models, with the use of the proposed method and with the use of the single average value as used in RDM, is compared against the results of the dynamic firing test for the propellant distribution samples. Finally, the influence of propellant variability on the ballistic performance parameters is shown, and the expected improvement over the modelling of assumed exact geometries in the conventional simulation code is assessed.

5.2 Closed vessel test

The samples tested by closed vessel traced the effect of geometric variability on the maximum pressure, dP/dt and dynamic vivacity. The dynamic vivacity in the closed vessel test was calculated according to STANAG 4115 as equation 11 and relative vivacity as follows:

$$RV = \frac{100}{R \times D} \qquad \textbf{Equation 38}$$

RV: Relative Vivacity

R: Reference

D: Each distribution

The reference is the vivacity value of the narrow normal distribution.

5.2.1 12.7 mm results and observations

Table 5.1 shows the results of the closed vessel test for propellant distribution samples for 12.7 mm. Max dP/dt and Max pressure were used to calculate dynamic vivacity.

Table 5.1 shows the narrow normal distribution, considered as a reference for relative vivacity to compare with the other distributions listed in Table 5.1. Therefore, the result of the relative vivacity shows that the gamma-skewed distribution is the highest, so the effect of the geometric variability observed a significant change in relative vivacity.

Table 5. 1: The results of the closed vessel test for 12.7 mm

Distribution:	Dynamic Vivacity	Relative Vivacity (%)	Max Pressure (MPa)	Max dP/dt (quickness)
Narrow normal distribution	3.25	100.00	227.18	87625
Normal distribution	3.22	98.99	223.86	86072
Gamma-skewed distribution	3.39	104.13	227.43	91679

5.2.2 5.56 mm results and observations

Table 5.2 shows the results of closed vessel tests for the propellant distribution samples from the 5.56 mm sample as the samples were prepared in Chapter 3. Max dP/dt and Max pressure were used to calculate dynamic vivacity.

Table 5.2 shows that the narrow normal distribution is considered as a reference for relative vivacity to compare with the other distributions listed in the Table. Therefore, the results of relative vivacity show that the normal distribution is highest, and the geometric variability observed a significant change.

Table 5. 2: The results of the closed vessel test for 5.56 mm

Distribution:	Vivacity	Relative Vivacity (%)	Max Pressure (MPa)	Max dP/dt (quickness)
Narrow normal distribution	4.66	100.00	243.83	138070
Normal distribution	4.76	102.15	246.58	141060
Gamma-skewed distribution	4.67	100.22	248.07	143600

5.3 Burning rate calculation

According to STANAG 4115, the measurement of the grains must be extremely precise and accurate to calculate the burning rate. The burning rate is calculated using the raw pressure data captured by the closed vessel along with time from the measured reaction (STANAG 4367, 2000).

Single average value was implemented according to RDM burning rate calculation, which assumed all the propellant grains have the same diameter size.

The raw pressure data obtained from the closed vessel test was used in the burning rate calculation. The burning rate calculation applied the proposed method and the single average value to calculate the coefficient and beta (exponent). Then, Vieille's equation was applied to calculate burning rate.

5.3.1 12.7 mm burning rate results and observations

As described in Chapter 4, all the grain diameters in a single average value burning rate were assumed to be 0.7 mm with a zero standard deviation. Besides, the average grain size was 0.7 mm for all distributions in the samples.

Very narrow normal distribution was assumed to have grain sizes very close to each other to verify the proposed method with the single average value method and to compare their results.

In addition, Table 5.3 shows that the burning rate results for narrow normal, very narrow normal and gamma distributions burnt in a shorter period than normal distribution, because the maximum pressure in the first three distributions is greater than the maximum pressure in the last distribution.

Table 5.3 shows the variation of burning rate results at two theoretical pressure values for the 12.7 mm propellant.

Table 5.3 lists the maximum pressure of the burning rate calculation as very close to the maximum pressure in the closed vessel (Table 5.1) for each distribution.

Table 5. 3: Burning rate parameters for 12.7 mm

Distribution:	Theoretical pressure MPa	Burning rate m/s	exponent	coefficient	Maximum pressure MPa
Normal	50	2.33	0.1450	1.3260	223
	230	2.91			
Narrow normal	50	2.29	0.1374	1.3390	226
	230	2.82			
Very narrow normal	50	2.30	0.1386	1.3379	226
	230	2.84			
Gamma-skewed	50	2.31	0.1378	1.3519	226
	230	2.86			
Single average value	50	2.30	0.1388	1.3376	226
	230	2.84			

Figure 5.1 shows the theoretical pressure versus burning rate results for the proposed method and single average value. The very narrow normal distribution curve matches the single average value curves because of the similarities in geometric grain size.

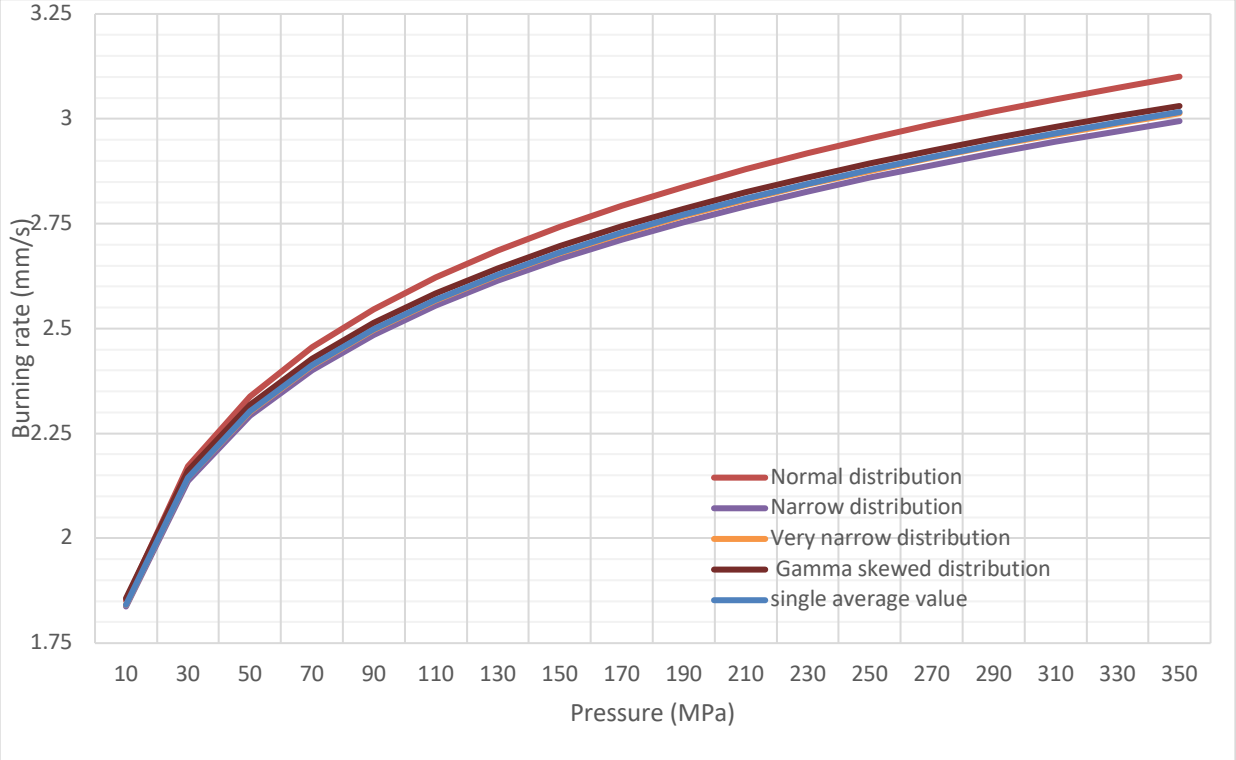

Figure 5. 1: Relevant burning rate parameters for PDF and single average value

5.3.2 5.56 mm burning rate results and observations

Table 5.4 briefly explains the results of the burning rate according to Vieille's equation mentioned in Chapter 1 with PDF and single average value. Table 5.4 lists the maximum pressure of the burning rate calculation as very close to the maximum pressure in the closed vessel (Table 5.2) for each distribution.

Other observations listed in Table 5.4 show the burning rate for gamma-skewed and normal distribution burning in a shorter period than narrow normal and very narrow normal, because the maximum pressure in the first two distributions is greater than

maximum pressure in the last two distributions. Figures 5.2 and 5.3 show the increase of burning rate with increasing pressure due to gas creation, as described in Section 4.4.2.

Table 5. 4: Burning rate for 5.56 mm

Distribution:	Theoretical pressure MPa	Burning rate m/s	exponent	coefficient	Maximum pressure MPa
Normal	50	3.21	0.2380	1.2665	245
	250	4.71			
Narrow normal	50	3.53	0.2683	1.2380	242
	250	5.44			
Very narrow normal	50	3.57	0.2710	1.2364	242
	250	5.52			
Gamma-skewed	50	3.05	0.2201	1.2892	247
	250	4.35			
Single average value	50	3.57	0.2712	1.2363	242
	250	5.53			

Figure 5.2 shows that the very narrow normal distribution curve matches the single average value curve, used according to RDM calculation. Therefore, the results of calculations of both are almost the same geometric grain size.

In addition, the exponent and coefficients differ with this distribution. These parameters explain the change in the burning rate curves in Figure 5.2 due to the presence of grain's geometric variability.

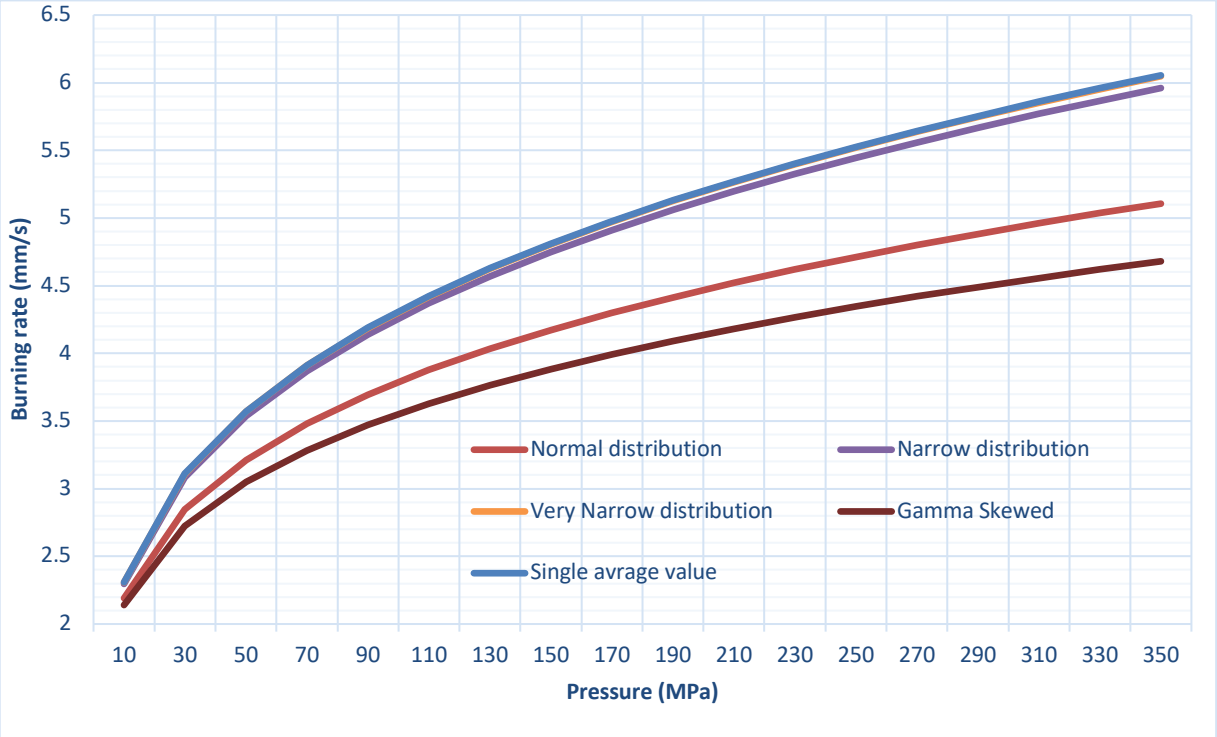

Figure 5. 2: Burning rate parameters for PDF and single average value

5.3.3 Discussion of the burning rate calculation

As mentioned earlier, the propellant samples in each calibre were tested using equal masses with the same composition.

The burning rate of the propellant is significantly influenced by the surrounding pressure. Each distribution type has a different grain size, which will result in different gas generation profiles and, thus, different pressure profiles. The outcome will therefore be a slight difference in the burning rate of each distribution. For instance, the maximum pressure at 5.56 mm is the highest value with a gamma-skewed distribution that has mostly small grains. Conversely, the maximum pressure at 12.7 mm is the lowest value with the gamma-skewed distribution that has mostly large grains. For both calibres, the very narrow distribution and single average value were similar, followed by the narrow distribution, due to the similarities in grain size.

5.4 Dynamic firing tests

As described in Chapter 3, gamma-skewed distribution for 12.7 mm had a larger grain diameter compared with the other distributions, but a smaller grain diameter for 5.56 mm.

The results show that gamma-skewed is the highest case mouth pressure with the fastest muzzle velocity. On the other hand, the narrow distribution, which had narrow geometric variability in 5.56 mm, had the lowest velocity as well as the lowest case mouth pressure. This result explains and highlights the effect of the fraction's grain size due to the similarity in size among the grains and the spread geometric grains. Therefore, the same amount of propellants in the same gun can lead to a better product by optimising geometry.

It has been noted from the 12.7 mm and 5.56 mm samples that narrow distribution, which is characterised by grains that are nearly identical in size, gives the lowest values in both pressure and velocity. This is because they burn while causing the projectile to move forward; however, all the propellant grains are completely burnt at

nearly the same time, before the projectile leaves the barrel, thereby causing the pressure to decrease. The pressure, in this case, does not continue to increase due to the complete combustion of the grains. On the other hand, grains of varying sizes take longer to burn, resulting in more continuity in the generation of both gas and pressure.

5.4.1 12.7 mm results and observations

The results in Table 5.5 show that for each type of distribution fired, three samples followed by the average and standard deviation are calculated for muzzle velocity and case mouth pressure. The standard deviation at narrow distribution is the smallest number amongst the other distributions.

Table 5. 5: Dynamic firing test results for 12.7 mm

Distribution:	Parameter	Muzzle Velocity	Case Mouth Pressure
	Unite	m/s	MPa
Normal	Average	871	341
	Standard deviation	17.3	24.3
Narrow normal	Average	858	318
	Standard deviation	3.1	2.3
Gamma-skewed	Average	877	353
	Standard deviation	25.7	36.4

In Figure 5.3, each dot represents an average of three shots.

The horizontal axis shows that the difference between the slowest velocity (858) and the fastest velocity (877) muzzle velocity is 19 m/s, which is a slight difference, even when taking into consideration the same composition of the propellant and the same charge loading. The results show that the gamma-skewed distribution has the highest case mouth pressure with the fastest muzzle velocity. On the other hand, the narrow distribution, which had narrow geometric variability, had the slowest muzzle velocity as well as the lowest case mouth pressure.

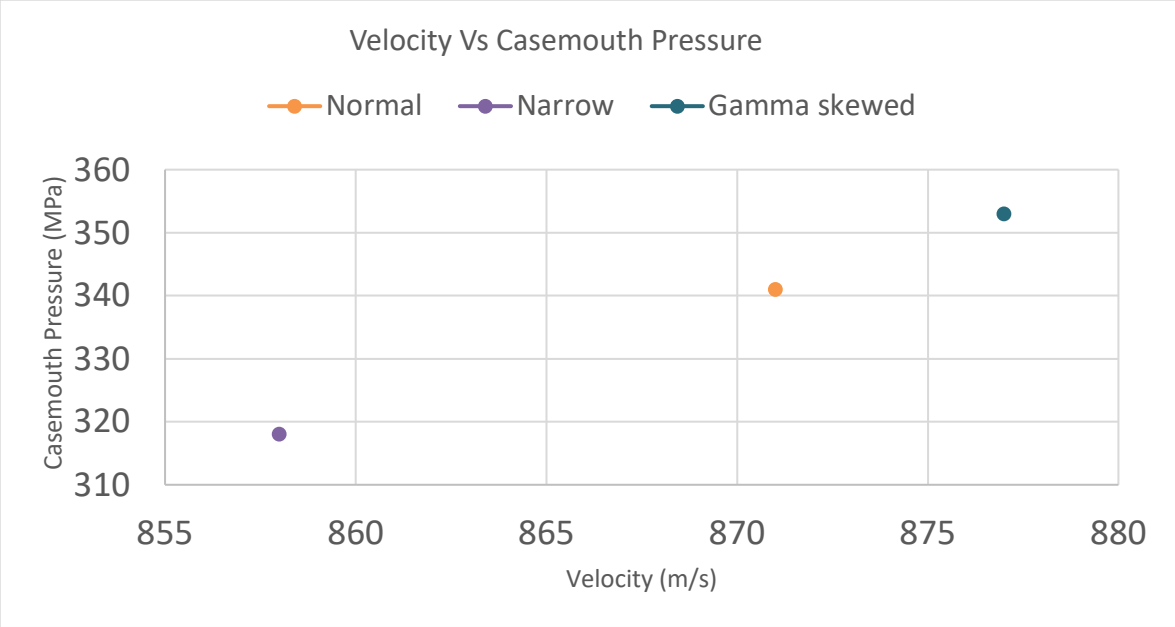

Figure 5. 3: Velocity vs case mouth pressure

5.4.2 5.56 mm results and observations

The dynamic firing tests for 5.56 mm show a comparison with propellant distribution samples.

As shown in Table 5.6, the average and standard deviation of velocity and case mouth pressure for three samples were calculated.

Table 5.6 shows that the standard deviation at narrow distribution is the smallest number among the other distributions.

Table 5. 6: The firing test results for 5.56 mm for propellant distribution samples

Distribution:	Parameter Unit	Muzzle Velocity m/s	Case mouth Pressure MPa
Normal	Average	935	397
	Standard deviation	3.1	1.2
Narrow normal	Average	932	387
	Standard deviation	0.6	0.6
Gamma skewed	Average	937	401

	Standard deviation	5.5	7.5

Figures 5.3 and 5.4 clearly show that the narrow distribution is the slowest in muzzle velocity due to the complete combustion of grains rapidly and at the same time. On the other hand, grains of varying sizes, such as in normal distribution and gamma-skewed distribution, take longer to burn, resulting in more continuity in the generation of gas and pressure.

The results of the dynamic firing test verify the effect of geometric variability among the grains on the performance (muzzle velocity and pressure) of the propellant.

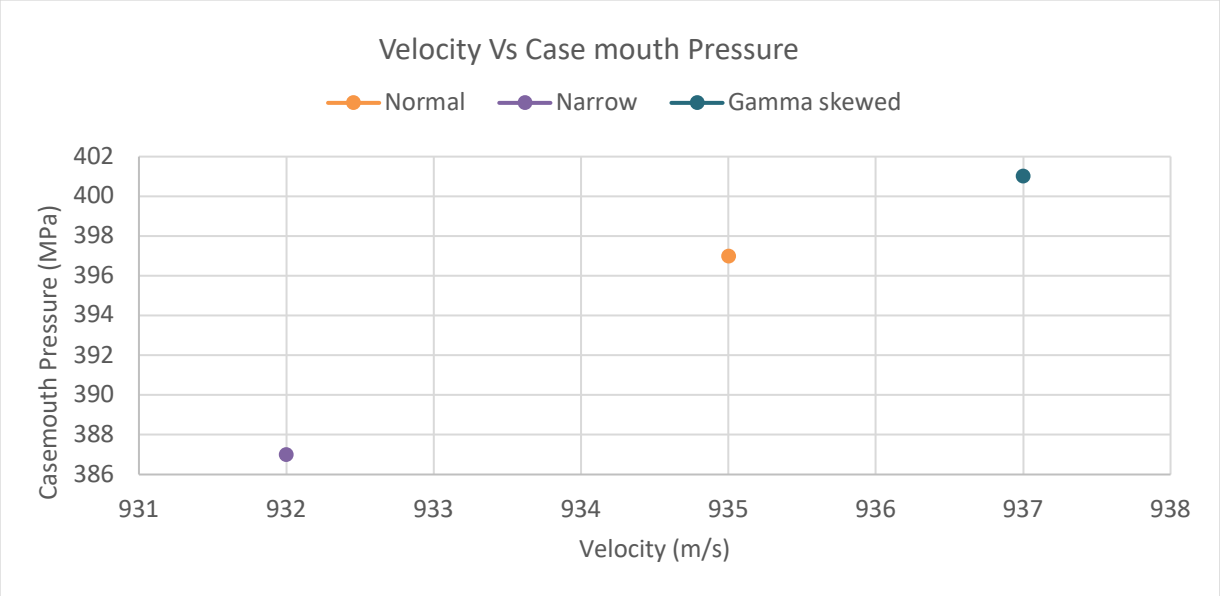

Figure 5. 4: Case mouth pressure vs velocity

5.5 IB simulation model

In this Section, the IB simulation model with PDF functions and single average value was implemented and compared with dynamic firing results to investigate the influence of propellant geometric variation for 12.7 mm and 5.56 mm ammunition propellant grains.

5.5.1 12.7 mm results and observations

Table 5.7 shows the results of the pressure and muzzle velocity for the IB simulation model with PDF vary between different distributions, which was proven in dynamic firing tests, while single average value cannot predict these variations. These results proved that the PDF simulation is more accurate than IB simulation with a single average value. Table 5.7 shows that the very narrow result is close to single average value, which is due to the similarity between the grain sizes.

Table 5. 7: Results of the dynamic firing test and IB simulation models for 12.7 mm

	Method	Pressure MPa	Normalised	Velocity m/s	Normalised
firing test	Normal distribution	341	1	871	1
	Narrow distribution	318	0.9325513	858	0.9850746
	Gamma-skewed distribution	353	1.0351906	877	1.0068886
IB simulation	Normal distribution	333	1	872	1
	Narrow distribution	325	0.976	870	0.998
	Very narrow distribution	322	0.967	868	0.995
	Gamma-skewed distribution	339	1.018	877	1.006
	Single average value	321	1	868	1

Figure 5.5 shows the normalized pressure with the dynamic firing test and PDF against the single average value (reference).

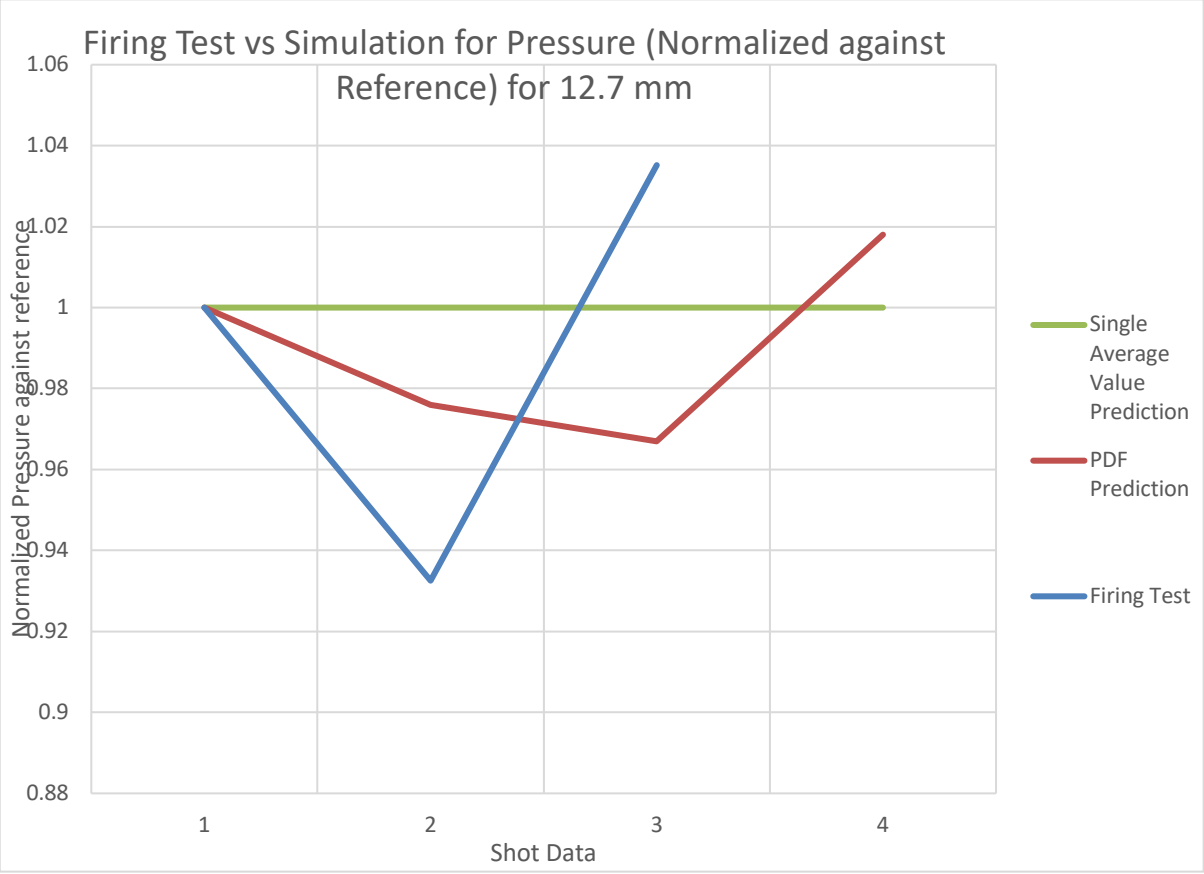

Figure 5. 5: IB simulation for pressure (normalised against reference) for 12.7 mm

Figure 5.6 shows the normalized muzzle velocity for each distribution against the single average value (reference).

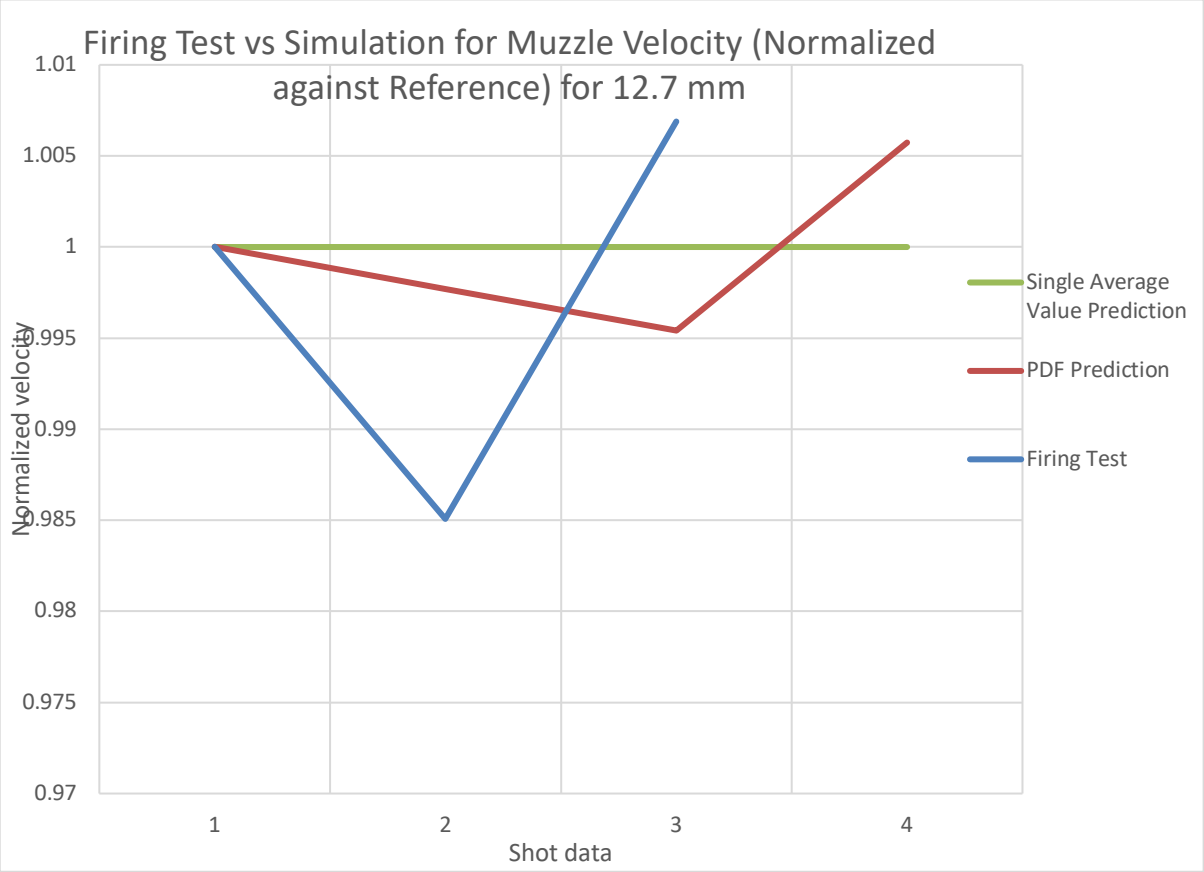

Figure 5. 6: IB simulation for PDF against single average value for 12.7 mm

5.5.2 5.56 mm results and observations

Table 5.8 shows the 5.56 mm results of PDF obtained by the IB simulation model for pressure and muzzle velocity normalised with the normal distribution, as well as the IB simulation model with single average value for pressure and muzzle normalised with its value.

Table 5. 8: Results of the dynamic firing test and IB simulation models for 5.56 mm

	Method	Pressure MPa	Normalised	Velocity m/s	Normalised
firing test	Normal distribution PDF	397	1	935	1
	Narrow distribution PDF	387	0.9748111	932	0.9967914
	Gamma-skewed PDF	401	1.0100756	937	1.002139
IB simulation	Normal distribution PDF	396	1	939	1
	Narrow distribution PDF	390	0.985	937	0.998
	Very narrow distribution PDF	388	0.980	935	0.996
	Gamma-skewed PDF	398	1.005	940	1.001
	Single average value	388	1	936	1

Table 5.8 shows that the standard deviation at very narrow distribution grains is the smallest number among the other distributions.

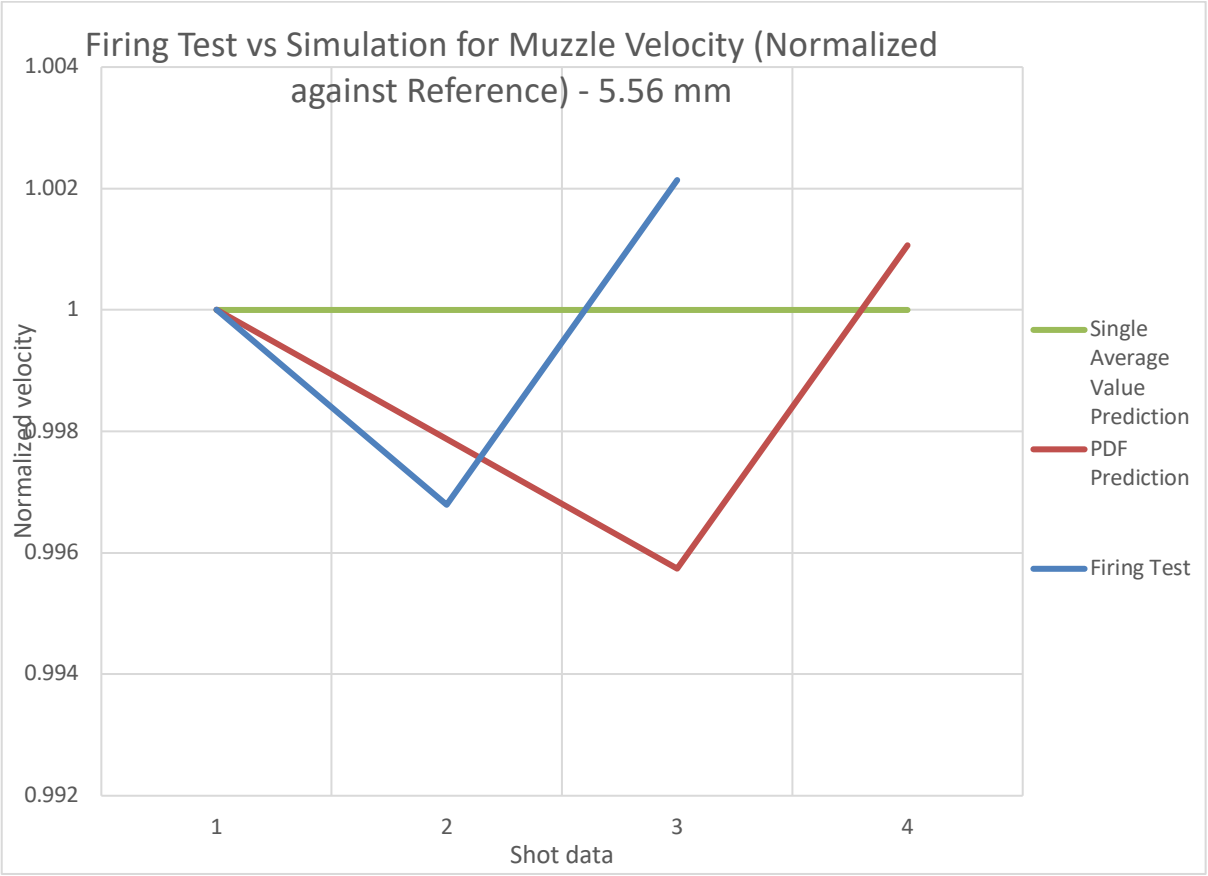

Figure 5. 7: IB simulation for muzzle velocity (normalised against reference) for 5.56 mm

In Figure 5.7, the normalised pressure curve of the PDF function is close to the single average value, but the results of the IB simulation model predict change with different geometric variability, which was proven by the dynamic firing test.

Figure 5.7 shows the comparison of normalized pressure curves between the IB simulation model with a single value and the IB simulation model with PDF against the dynamic firing test.

Both the IB simulation model with PDF and the samples used for the dynamic firing test had different geometric variability. Therefore, the results vary in contrast with the IB simulation model with single average value, which cannot predict this.

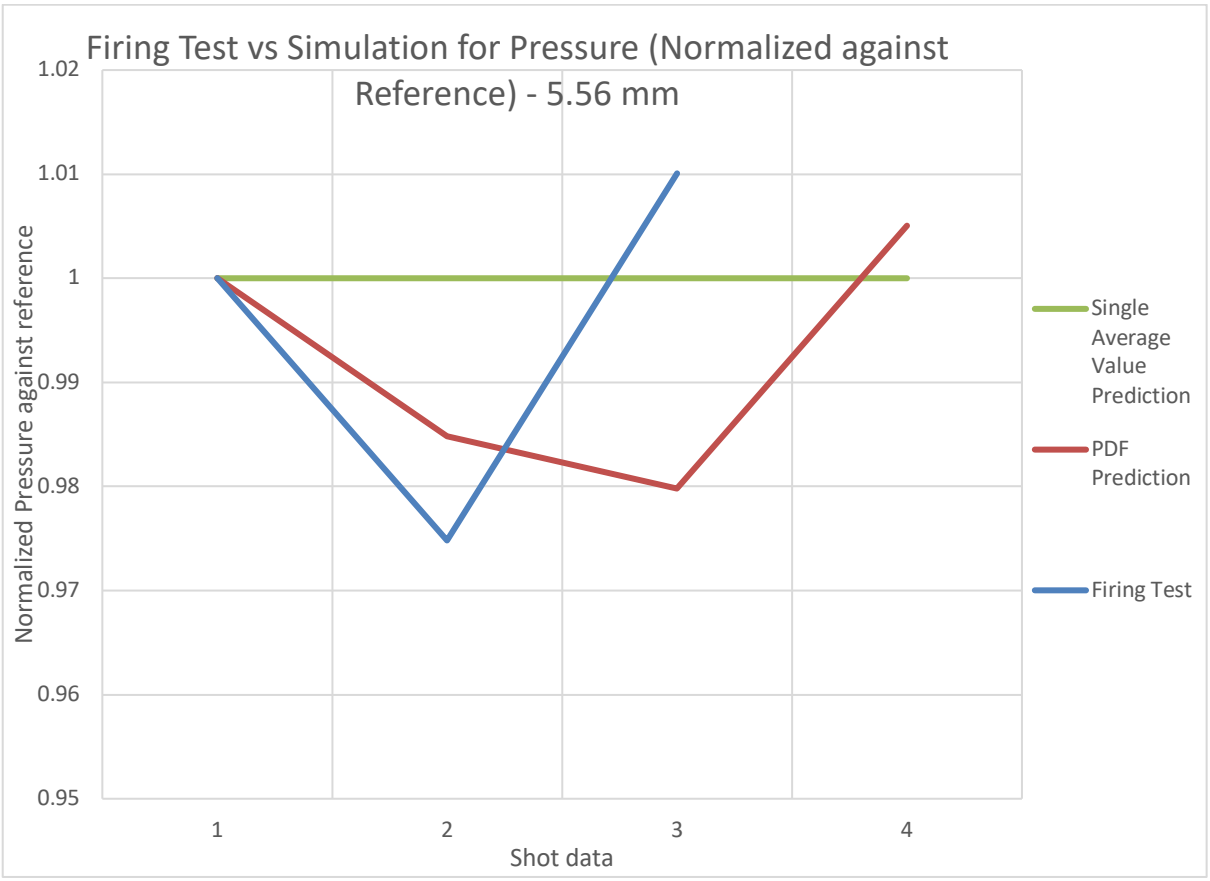

Figure 5. 8: IB simulation for pressure (normalised against reference) for 5.56 mm

In Figure 5.8, the normalised curve of the velocity of the PDF is closer to the dynamic firing data than the single average value.

Figure 5.7 and Figure 5.8 show that the IB simulation model with PDF function predicts the influence of included variabilities of geometric grains on pressure and muzzle velocity. Therefore, this shows the accuracy of the IB simulation model with PDF methods.

5.6 Conclusions

This Chapter compared the results of different geometric grain variabilities for ball powder propellant samples. The influence of the propellant grain geometric variability on gas generation was characterised. The propellant performance was described by the dynamic vivacity, burning rate, pressure and muzzle velocity.

Closed vessel ballistics is closely tied to the actual geometry of the propellant. Therefore, the geometry should be specified as closely as possible to reality.

The vivacity shows the gas generation profile of the propellant grains. Because the propellant has the same chemical composition and because the mass is similar between the samples, the burn rate of the sample is not expected to differ. However, because the geometry of the samples does differ slightly, the gas generation profile is also expected to show slight differences. As a result, the burning rate will differ.

The results of the dynamic firing tests for grains of different diameters confirmed that these differences in pressure influence the muzzle velocity at both 12.7 mm and 5.56 mm. This influence was predicted by the IB simulation model with PDF, while the single average value does not take it into account.

These findings indicate more reliability for the IB simulation model with PDF than for the IB simulation model with the single average value method.

The experimental result for 12.7 mm and 5.56 mm, conducted in a closed vessel and dynamic firing tests, confirmed the importance of propellant grain variability. This variability should be taken into consideration during implementation by incorporating the burning rate calculation and IB simulation models for more realistic results.

In conclusion, this study has developed and demonstrated an improved method for calculating and simulating solid propellant gas delivery manipulating conventional IB simulation models.

CHAPTER 6: CONCLUSIONS

6.1 Conclusion

The following objectives was achieved:

- The geometric variability distribution with relevant PDF functions incorporated into IB simulation model and burning rate calculation.
- A single average value baseline IB simulation model and burning rate calculation has been established.
- This study explained the methodology of indirect measurement of Ball Powder propellant grains and characterised the geometric variability between the grains by sieving process to create propellant distributions samples;
- Tested the propellant distributions samples by closed vessel and dynamic firing test;
- Developed a method and software in order to calculate the burn rate of propellant based on PDF functions against single average value;
- Tested and verified an IB simulation model with PDF functions against single average value;
- Studied the influence of geometric variability in comparison to single average value against PDF functions by conducting relevant IB simulations.

In the previous Chapter the results of burning rate calculation for single average value are verified against the results of burning rate calculation for PDF functions. And the outputs of IB simulation model for both PDF functions and single value are verified against dynamic firing test.

The result of IB simulation model with PDF functions is close to the results of dynamic firing test show that than the IB simulation model with single average value. Thus, the inclusion of geometric variability between the grain sizes within the IB simulation adds realism to the simulation.

By including the variability on the geometric of propellant grains within IB simulation model, the results proved more accurate than the simulation model assuming they are exactly the same.

The results of dynamic firing tests show that geometric variability affected the propellant performance in terms of pressure and muzzle velocity for ball powder. Testing ball powders with the same composition and mass, but with variability in the grain size, obtained different results with the dynamic firing test. The influence of grain size geometric variability was characterised and demonstrated in this study.

This study explains, by experimentation, the importance of the effect of grain geometry variability represented by assumption of geometric variability distribution as an input in the IB simulation model and burning rate calculation.

6.2 Future research

For future research, the method used in this study could be applied to other propellant shapes. Additionally, future research could attempt to simulate variability among the length and perforation diameter of single perforation grains and multi perforations grains.

It is also important to consider measurement methods for grain geometry and to generalize input formulation description of PDF's for IB Simulation Models.

6.3 Final conclusion

The variability of the propellant grain geometry, represented by PDF functions, was applied to develop the IB simulation model and burning rate calculation. In this way, it was demonstrated that the method adds more realism to the propellant evaluation.

REFERENCES

Agrawal, J. P. (2010). *High Energy Materials: Propellants, explosives and pyrotechnics*. Wiley-VCH Verlag & KGaA, Weinheim.

Bailey, A. & Murray, S. G. (1989*). Explosives, Propellants and Pyrotechnics.* London: Brassey's.

Ball A. M. (1960). *Engineering design handbook explosives series solid propellant part 1*, U.S.Army Research Office-Durham, North Carolina

Baschung, B. & Grune, D. (2000). *The closed vessel: Still an essential experimental device for interior ballistics in the future.* Proceedings of the European Forum on Ballistics of Projectiles, Saint Louis.

Botelho, F. D., Galante, E. B. F., & Mendes, Á. J. B. (2015). Characteristics and manufacture of spherical smokeless powders. *Journal of Aerospace Technology and Management*, *7*(4), 398-403. doi: 10.5028/jatm.v7i4.466

Carlucci, D. E. & Jacobson, S. S. (2008). *Ballistics: Theory and design of guns and ammunition*. Taylor & Francis Group, LLC, Boca Raton.

Horst, A. W. & Nusca, M. J. (2006). *The Charge Designer's Workbench: A range of interior ballistic modelling tools*.

Joyce, D., 2016. *Common probability distributions Math 217/218 Probability and Statistics*. Clark University

Kubota, N. (2002). *Thermochemical Aspects of Combustion. Propellants and Explosives*. doi: 10.1016/j.mseb.2010.10.009 Wiley-VCH Verlag & KGaA, Weinheim.

Johannes, M. (2019). *Dynamic firing tests* [Personal interview]. 15 Mar., Somerset West.

Oberle, W. F. (2001). *Dynamic vivacity and its application to conventional and electrothermal-chemical (ETC) closed chamber results*.

Pocock, M., Neill, J., & Guyott, C. (2001). *Factors affecting the accuracy of internal ballistics, including the simulation of propellant motion*. Forum American Bar Association, (May).

Pocock, M., Locking, P., & Guyott, C. (2003). *Effect of statistical variation in grain geometry on internal ballistics modelling*. Frazer-Nash Consultancy Ltd and Bae Systems, Ro Defence, UK.

Poulsen, T. (2010). *Introduction to Chemistry.* CK-12 Foundation.

Rawle, A., Limited, M. I., Park, E. B., & Road, G. (2003). Basic Principles of Particle. Surface Coatings. *International Part A Coatings Journa*l, *44*.

Rheinmetall Denel Munition RDM Handbook, (2016), Potchefstroom.

Rheinmetall Denel Munition RDM Handbook, (2017), Somerset West.

Rodrigues, R. L. B., Castier, M., & Peixoto, F. C. (2006). Closed vessel experiment modelling and ballistic parameter estimation of gun propellants for lifetime prediction. *Latin American Applied Research*, *36*(4).

Rousseau. P.G. Notes, C., & Engineering, F. O. F. (2013). Thermal-fluid systems modelling, NWU. Potchefstroom

Schabort V. (2017) [personal interview]. 4 May., Somerset West.

STANAG 4115. (Edition 2). (1997). Definition and determination of ballistic properties of gun propellants.

STANAG 4367. (Edition 2). (2000). The thermodynamic interior ballistic model with global parameters.

STANAG 4367. (Edition 3). (2009). The Thermodynamic interior ballistic model with

global parameters.

STANAG 4400. Land (Edition 1) (Amendment 1). (1993). Derivation of thermochemical values for interior ballistic calculation.

STANAG AOP 7. (Edition 2). (2003). Manual of data requirements and tests for the qualification of explosive materials for military use.

Tenney L. (1943). T*he Chemistry of Powder and Explosive*.

Walpole, R., Myers, R., Myers, S. & Ye, K. (2012). Probability and Statistics for Engineers and Scientists (9th Edition). Retrieved from: . http://fac.ksu.edu.sa/sites/default/files/probability_and_statistics_for_engineers_and_scientisst.pdf

Wiehahn C. (2018). Thermochemical properties [Personal interview]. 13 Sep., Somerset West.

Yildirim, F. (2012). *Optimal propellant grain geometry design for large calibre projectiles*, Belgrade, Defensive Technologies.

APPENDIX A

Figure 1: This picture shows the geometric variability among the grains in the 12.7 mm sample

Figure 2: Setup of the sieves to prepare the ball powder samples

Figure 3: Instrument setup for 12.7 mm sample

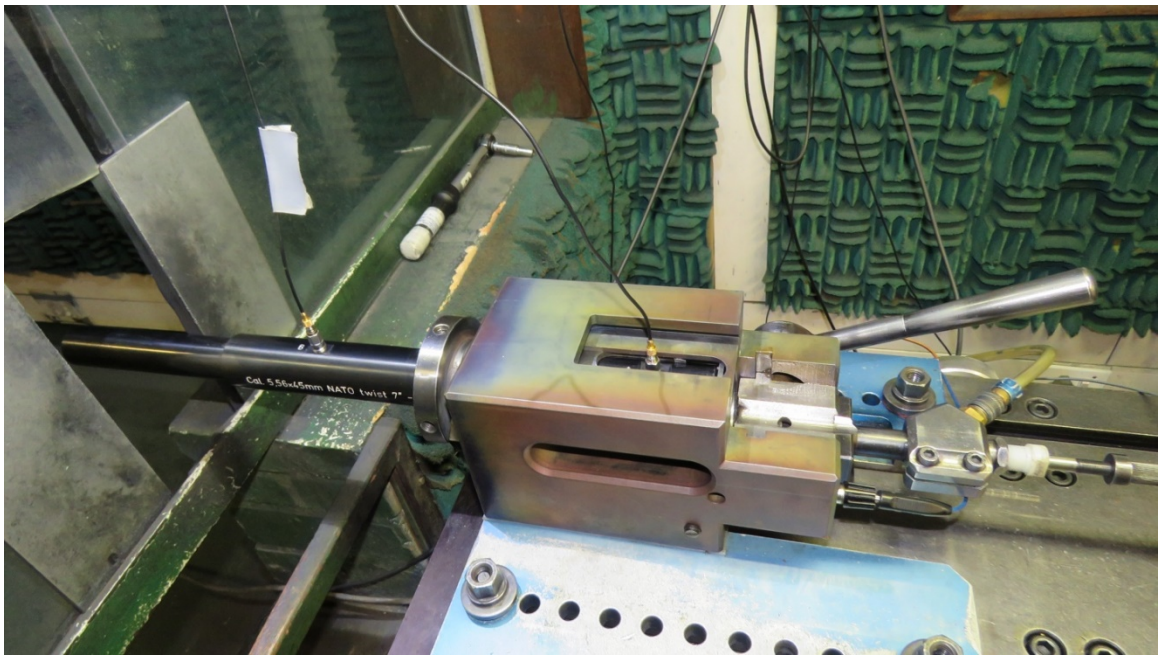

Figure 4: Instrument setup for 5.56 mm sample

Figure 5: The piezoelectric pressure sensor

APPENDIX B

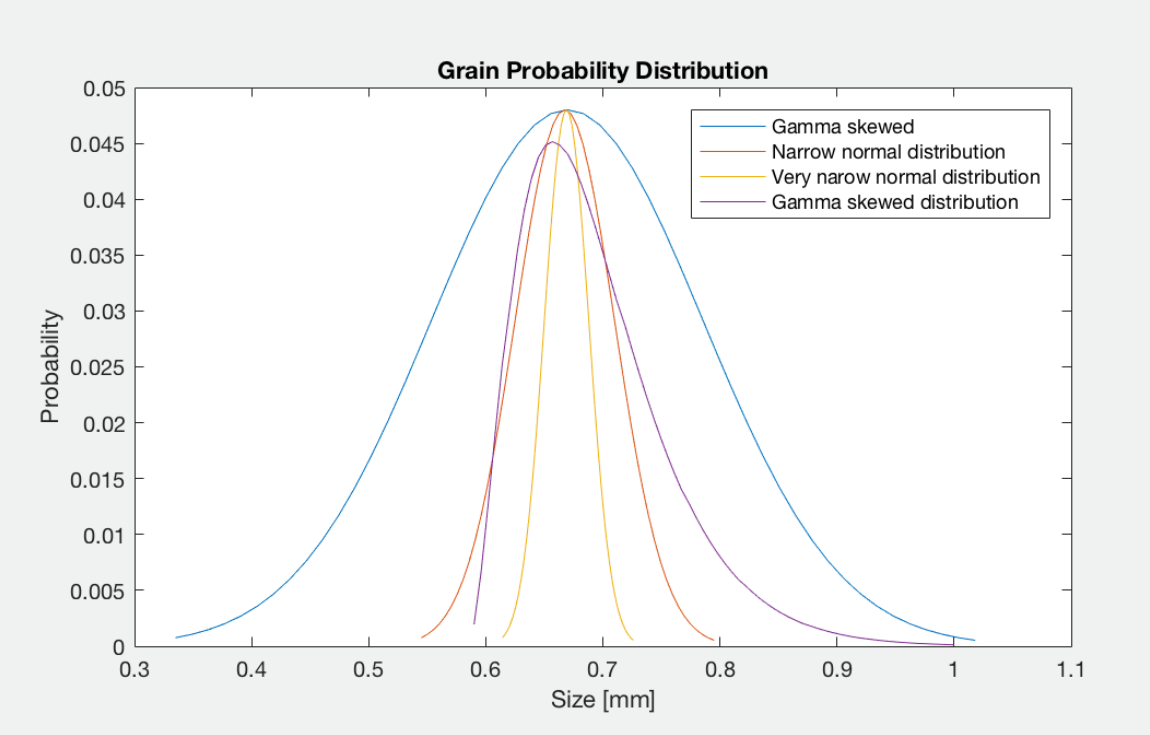

Figure 6: Propellant grains diameter sizes with different distributions

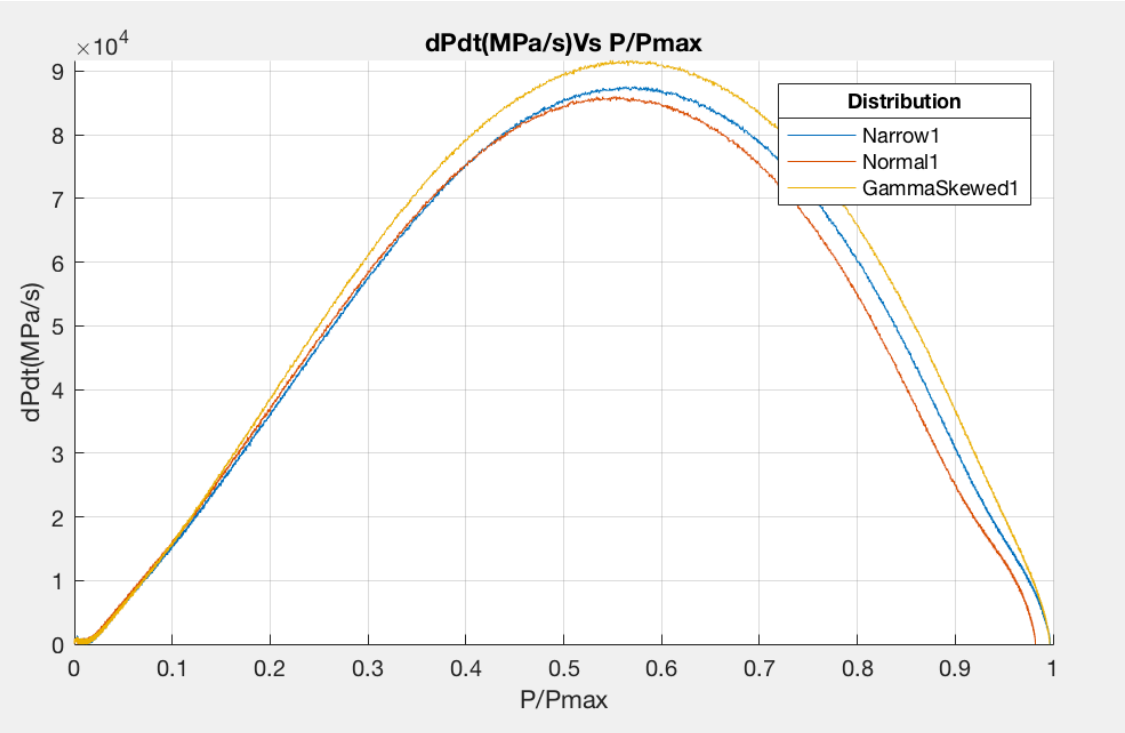

Figure 7: Closed vessel curves for different distribution in 12.7 mm

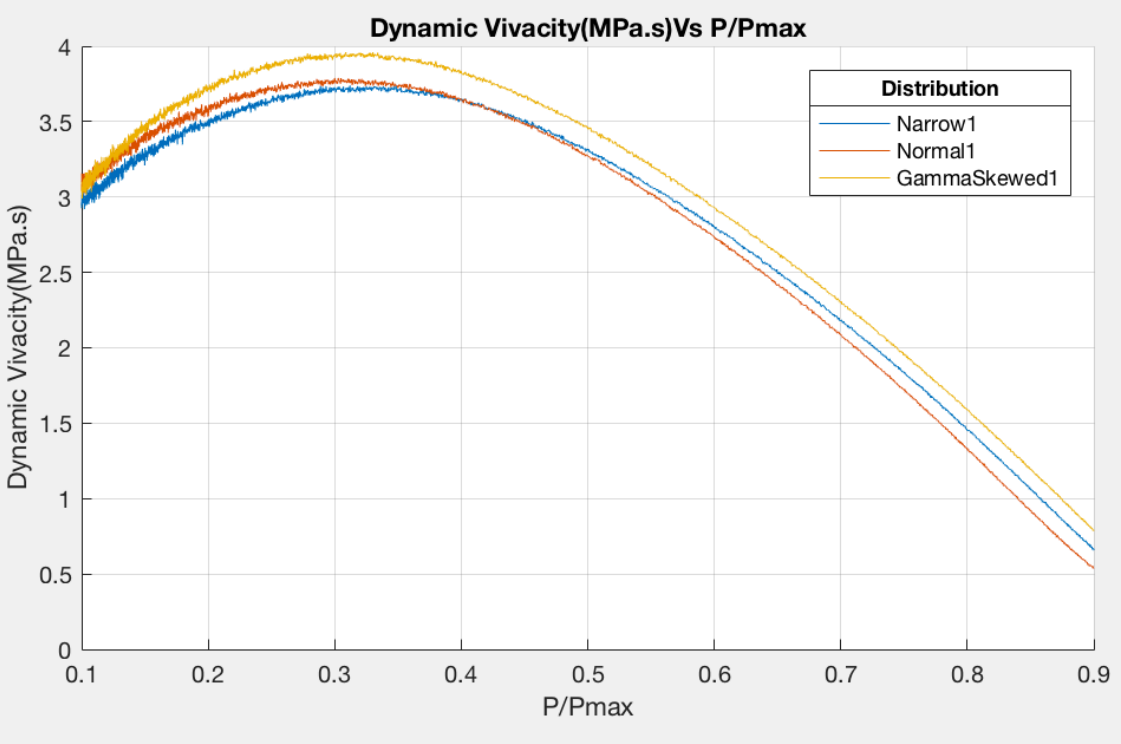

Figure 8: Closed vessel curves for different distribution in 12.7 mm

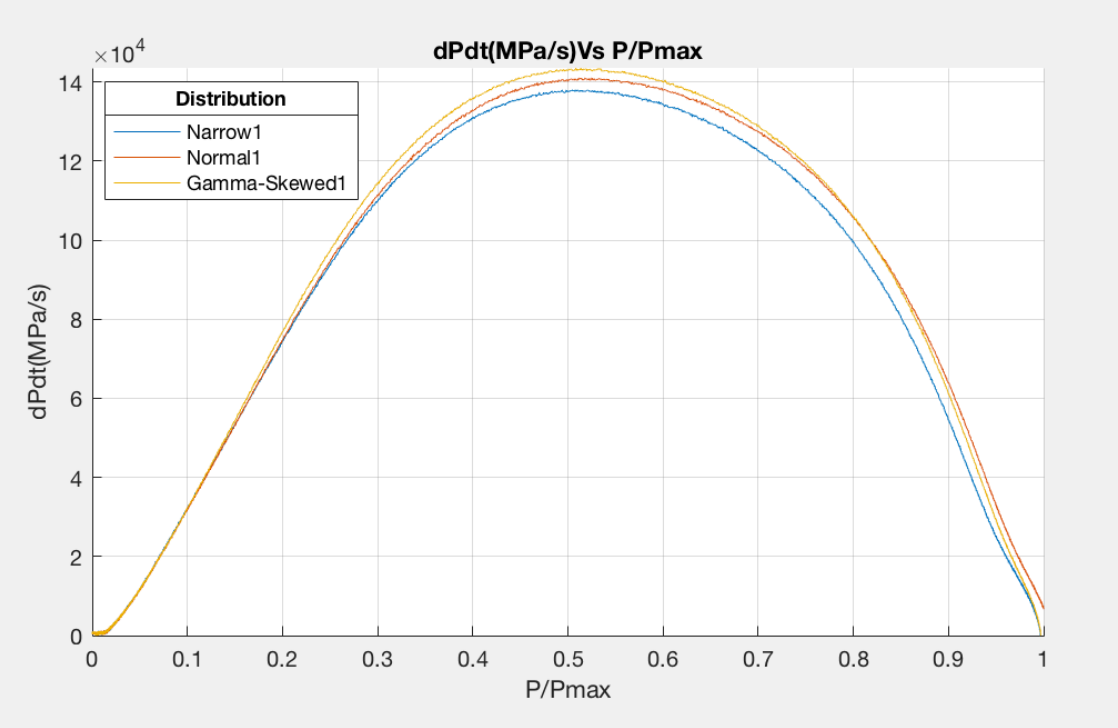

Figure 9: Closed vessel curves for different distribution in 5.56 mm

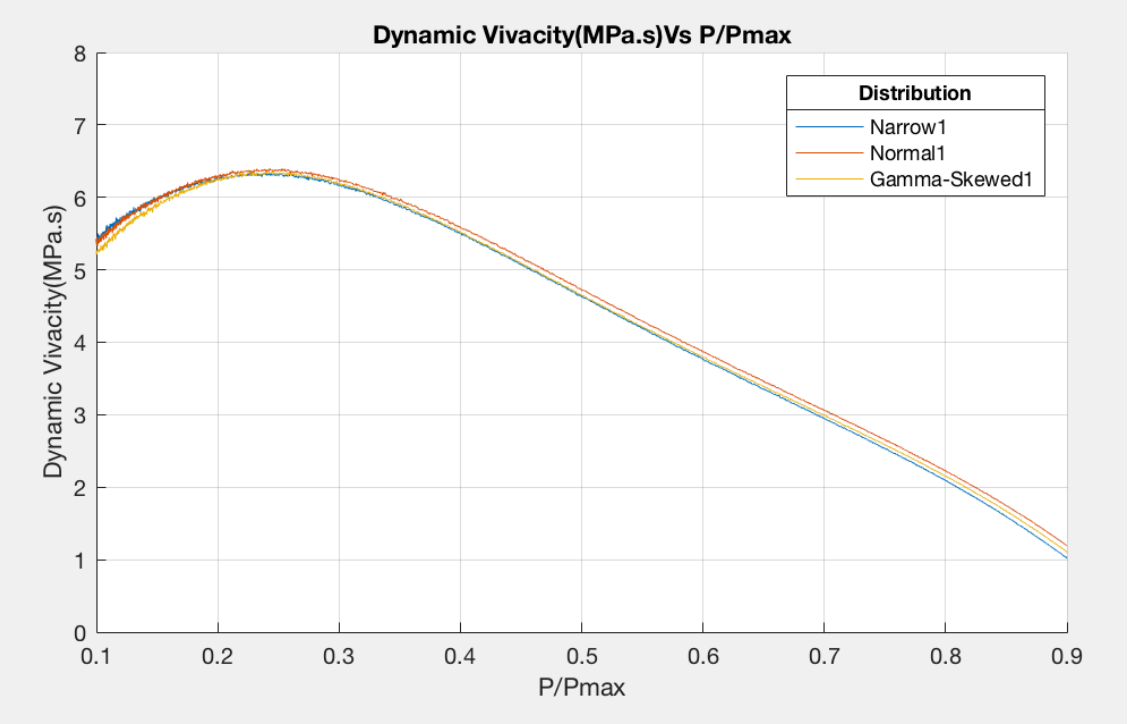

Figure 10: Closed vessel curves for different distribution in 5.56 mm

APPENDIX C

Laboratory Test and Thermochemical Properties

Full chemical analysis:

Table A1: Propellant ingredients for 12.7 mm and 5.56 mm

Propellant ingredients	First Composition	Second Composition
Chemical ingredients	12.7 mm	5.56 mm
Nitrocellulose (%)	79.3	83.67
Nitro-glycerine (%) Plasticiser	8.57	9.47
Dibutyphalate (%) (DBP) Plasticiser	8.35	4.27
Diphenylamine (DPA) Stabiliser	0.86	0.76
N-Nitroso-Diphenylamine (NNO-DPA) Stabiliser	-	0.61
Calcium Carbonate	0.12	0.09
Potassium Nitrate	0.73	0.46
Tin Dioxide	1.03	-
Graphite	0.13	0.17
Water and volatile matter	1.13	1.04
Dust and foreign matter	0.1	0.02

The instruments used in full chemical analysis:

- High-Pressure Liquid Chromatography (HPLC)
- Gas Chromatography (GC)
- These two processes could detect NG, EC, DPA, DBP, NNo. DPA and DEP
- Atomic Absorption Spectrometric Spectrophotometry to detect Potassium Sulphuric K_2SO_4 in the samples
- Spectroscopy Near Infrared (NIR)

Thermochemical Properties

Table A2 Thermochemical Properties for all samples

Thermochemical Properties	First Composition	Second Composition
	12.7 mm	5.56 mm
Heat of explosives	3336.3 joules/g	3729 joules/g
Oxygen Balance	- 45.26%	- 37.62%
Gamma	1.5628	1.5321
Kappa (=Cp/Cv)	1.2583	1.2417
Specific Energy	934.3 J/G	1028.3 J/G
Temperature	2586.1 K	2980 K

Appendix D:

Dynamic Firing Test Results for 12.7 mm:

Normal distribution

	Velocity	Case mouth Pressure
	m/s	MPa
1	880	354
2	851	313
3	882	356
Average	871	341
Stander deviation	17.3	24.3

Narrow distribution

	Velocity	Case mouth Pressure
	m/s	MPa
1	855	317
2	859	317
3	861	321
Average	858	318
Stander deviation	3.1	2.3

Gamma Skewed distribution

	Velocity	Case mouth Pressure
	m/s	MPa
1	892	374
2	847	311
3	891	374
Average	877	353
Stander deviation	25.7	36.4

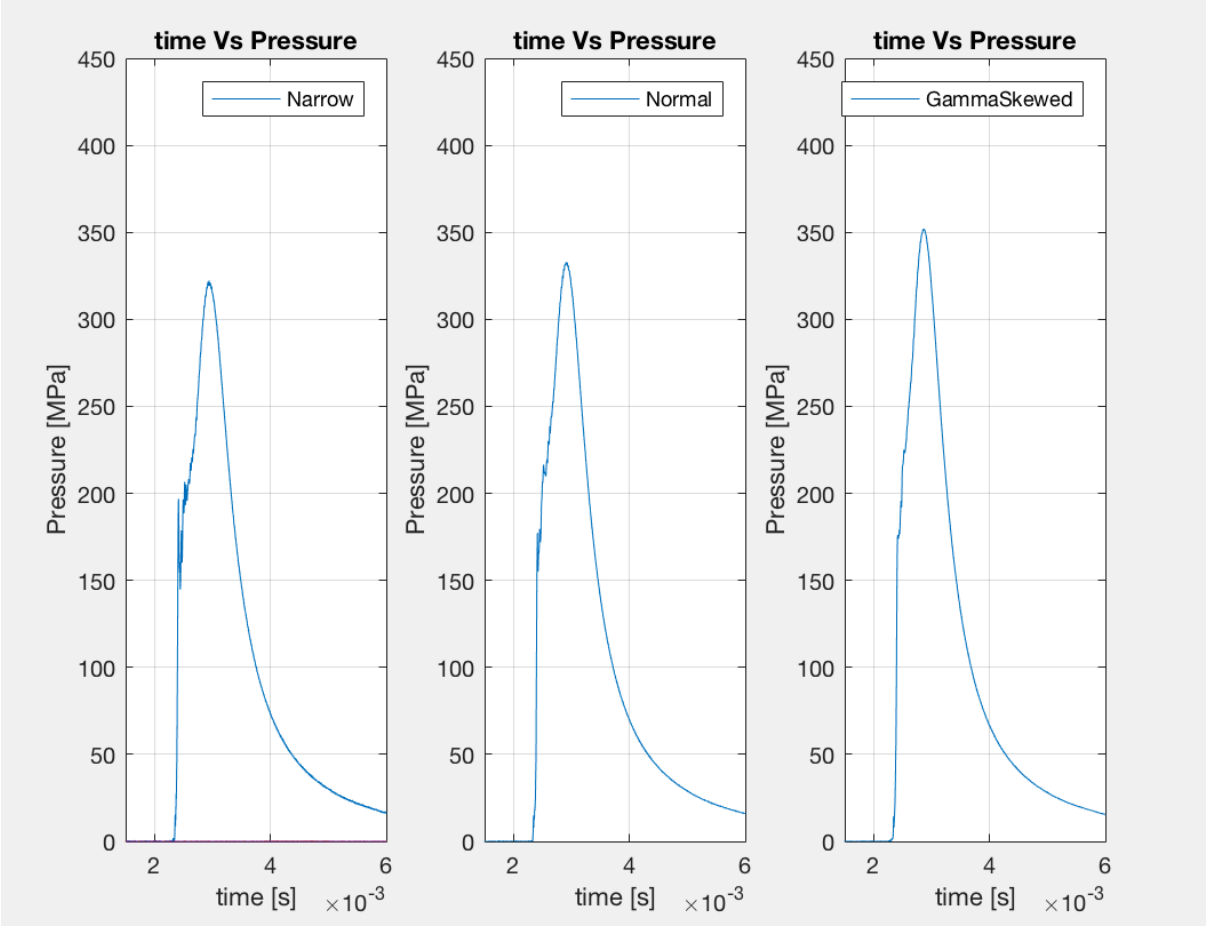

Figure 11: Pressure-time curves of dynamic firing test for 12.7 mm

Dynamic Firing Test Results for 5.56 mm:

Normal distribution

	Velocity	Case mouth Pressure
	m/s	MPa
1	938	398
2	934	396
3	932	396
Average	935	397
Stander deviation	3.1	1.2

Narrow distribution

	Velocity	Case mouth Pressure
	m/s	MPa
1	932	387
2	932	388
3	931	387
Average	932	387
Stander deviation	0.6	0.6

Gamma skewed distribution

	Velocity	Case mouth Pressure
	m/s	MPa
1	931	393
2	942	408
3	937	401
Average	937	401
Stander deviation	5.5	7.5

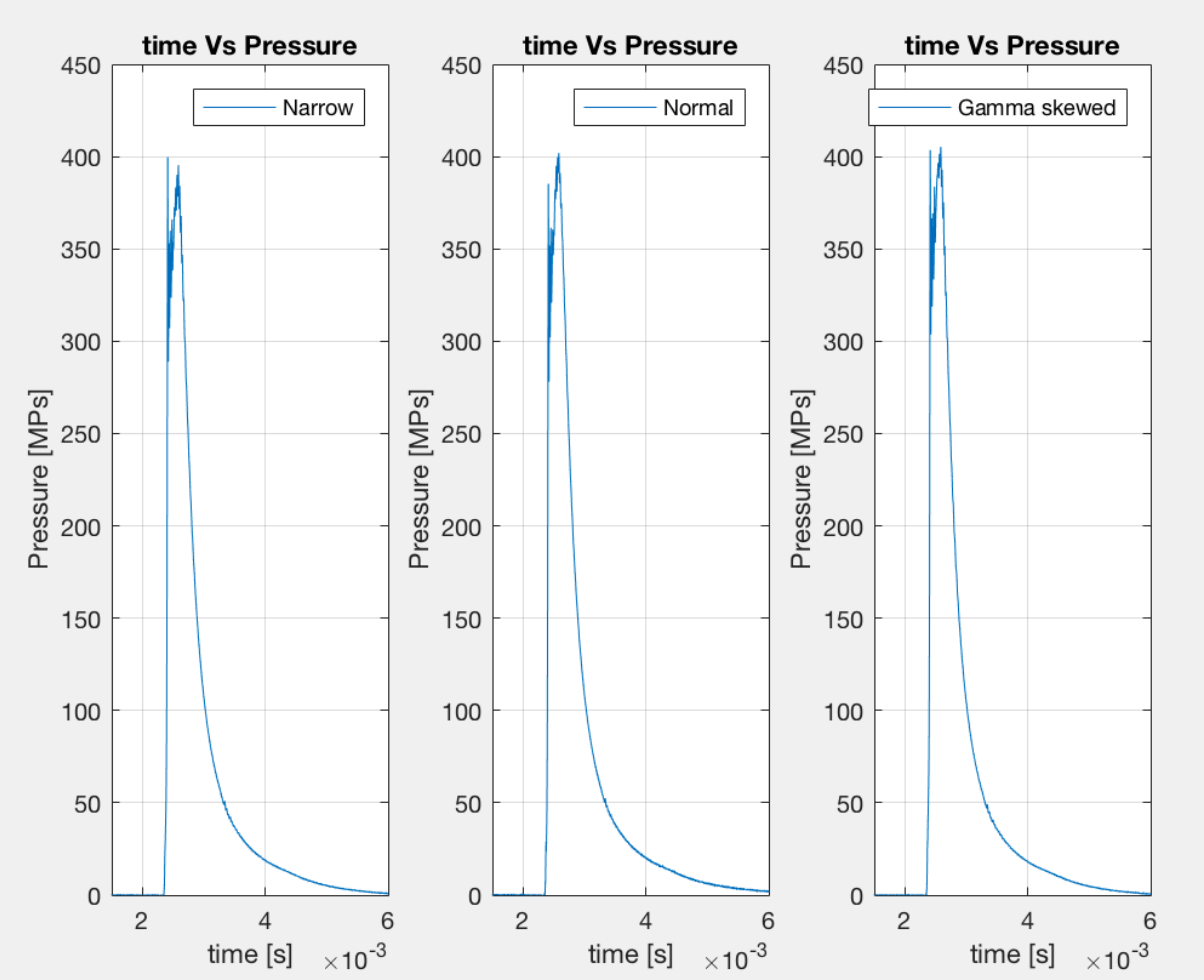

Figure 12: Pressure-time curves of dynamic firing test for 5.56 mm

Appendix E:

Burning rate calculation and IB simulation model

Form Function Code according to STANAG 4367 for both 12.7 mm and 5.56 mm adapted from RDM codes was used in this study for burning rate calculation and IB simulation Code:

```
function [GrainVolume GrainArea] = FormIBSim(d,PropGeom,n)
% Form - To call appropriate form function
% d - Distance burnt in [m]
% PropGeom Structure:
%  .Type   Grain Type: 0-Ellipsoid,1-Cord,2-Tube,3-Ball
%  .a  Ellipsoid half width
%  .b  Ellipsoid hag Length
%  .c  Ellipsoid half height
%  .L  Grain Length
%  .D  Grain Diameter (Ball, Tube or Cord)
%  .P1 Perforation diameter
%  All in [m] units
%
%  Function return Grainvolume and Grain burn area
%
 switch PropGeom.Type(n)
  case 0
  [GrainVolume GrainArea] = Ellipsoid(d,PropGeom,n);
  case 1
  [GrainVolume GrainArea] = Cord(d,PropGeom,n);
  case 2
  [GrainVolume GrainArea] = Tube(d,PropGeom,n);
  case 3
  [GrainVolume GrainArea] = Ball(d,PropGeom,n);
 end
end

function [V A] = Ball(d,Geom,n)
% Ball geometry
%  Input:
%  d - distance burnt [m]
%  Geom.D - Grain diameter [m]
%  Output:
%  V - Volume [m3]
%  A - Area   [m2]

 r = (Geom.D(n)/2.0-d);   % Radius

 if(r > 0.0)
   V = 4/3*pi*r*r*r;
   A = 4*pi*r*r;
 else
   V = 0.0;
   A = 0.0;
 end
 end
```

```
function [V A] = Ellipsoid(d,Geom,n)
% Ellipsoid geometry
%  Input:
%  d - distance burnt [m]
%  Geom.a - Grain length [m]
%  Geom.b - Grain width  [m]
%  Geom.c - Grain height [m]
%  Output:
%  V - Volume [m3]
%  A - Area   [m2]
 a = Geom.a(n)-d;
 b = Geom.b(n)-d;
 c = Geom.c(n)-d;

 if(a > 0.0 && b > 0.0 && c > 0.0)
   V = 4/3*pi*a*b*c;
   A = 4*pi*(((a*b)^(1/6)+(a*c)^(1/6)+(b*c)^(1/6))/3)^(1/1.6);
 else
   V = 0.0;
   A = 0.0;
 end
 end

function [V A] = Cord(d,Geom,n)
% Cord or Flake geometry
%  Input:
%  d - distance burnt [m]
%  Geom.D - Cord/Flake Diameter [m]
%  Geom.L - Cord length of Flake thickness[m]
%  Output:
%  V - Volume [m3]
%  A - Area   [m2]
 r = (Geom.D(n) - 2*d)/2.0;
 L = Geom.L(n) - 2*d;
  if(r > 0.0)
   V = 2*pi*r^2*L;
   A = 2*pi*r^2 + 2*pi*r*L;
  else
   V = 0.0
   A = 0.0
  end

 end

function [V A] = Tube(d,Geom,n)
% Single Perf geometry
%  Input:
%  d - distance burnt [m]
%  Geom.D - Tube Diameter [m]
%  Geom.L - Tupe Perforation diameter [m]
%  Output:
%  V - Volume [m3]
%  A - Area   [m2]
 r1 = (Geom.P1(n)+2*d)/2.0;    % Inside radius
 r2 = (Geom.D(n)-2*d)/2.0;     % Outside radius
 L = Geom.L(n)-2*d;

 if((r2-r1) > 0.0)
```

```
    V = 2*pi*L*(r2^2-r1^2);
    A = 2*pi*(r2^2 - r1^2) + 2*pi*r1*L + 2*pi*r2*L;
  else
    V = 0;
    A = 0;
  end

end
```

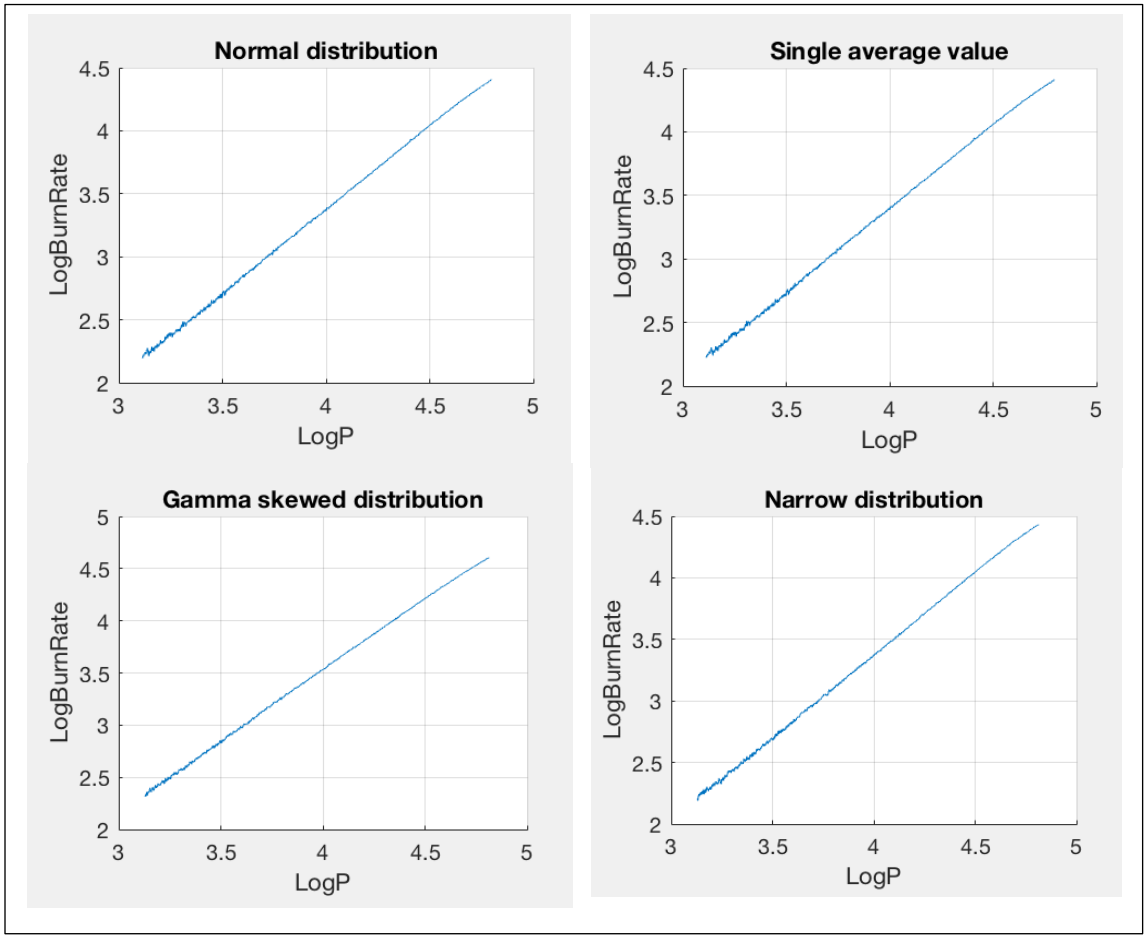

Figure 13: Log burning rate versus log pressure for 12.7 mm

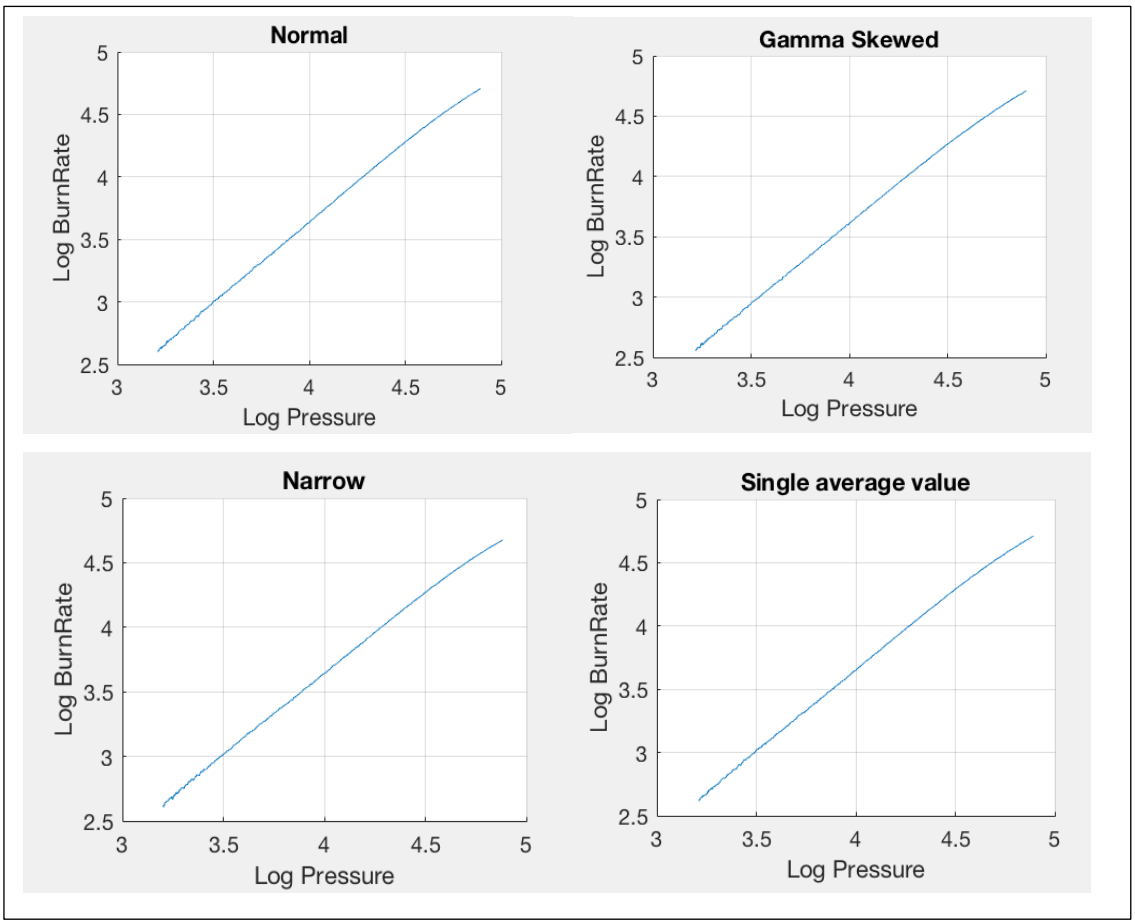

Figure 14: Log burning rate versus log pressure for 5.56 mm

The required inputs inserted via IB simulation model to simulate a basic gun IB cycle according to STANAG 4367 (Edition 2) for 12.7 mm (adapted from RDM IB simulation codes):

```
clc;
clear all;
%close all;

% Global Data Definition Section
% Gun and projectile parameters
global ChVolume;                    % (Input) Chamber volume
global ProjMass;                    % (Input) Projectile Mass
global GrooveLength;                % (Input)
global GrooveDiam;                  % (Input)
global LandDiam;                    % (Input)
global GLRatio;                     % (Input)
global BarrelDiamSq;                % Calculated according to STANAG
```

```
global RiflingTwist;              % (Input)1 360deg Rotation in Number of
calibres (Input)
global RecoilMass;                % (Input) Recoil part total mass  (Input)
global RecoilResistance0;         % (Input) Initial threshold recoil
resistance [N]  (Input)
global RecoilResistance;          % (Input) Cycle Recoil resistance [N]
(Input)
global XR;                        % (Input) Resistance model - x    [m]
(Input)
global PR;                        % (Input) Resistance model - Pr   [MPa]
(Input)
global Presist;

% STANAG adjustment factors
global Fbr;                       % (Input) Bore resistance factor
global Fr;                        % (Input) Burn Rate adjustment factor
global Fft;                       % (Input) Force constant temperature
factor
global Ft;                        % (Input) Burn rate temperature factor

% Heat Loss Input values
global h0;                        % (Input) Heat Transfer Coeff of air
global WallThickness;             % (Input) Nominal wall thickness
global CpWall;                    % (Input) Wall material heat capacity
global RhoWall;                   % (Input) Wall material density
global WallT0;                    % (Input) Wall initial temperature
global TWall;                     % (Input) Wall initial temperature
global fFriction;                 % (Input) Wall Preheat factor

% State Vector arrays (1xn variables)
global TimeStep;       % Time step size (Input)
global Time;           % Cycle Time in [s]
global Z;              % Propellant fraction burnt for each propellant and
entire cycle(2d array) - 1st index: cycle no, 2nd index: propellant no
global BurnDist;       % Propellant Burn Distance vector (for each
propellant)
global BurnRate;       % Propellant Burn Rate (for each propellant)
global X;              % Projectile position [m]
global V;              % Projectile velocity [m/s]
global A;              % Projectile acceleration [m/s/s]
global Pbr;            % Breech Pressure
global Pc;             % Chamber average pressure
global Pba;            % Projectile Base Pressure
global Egas;           % Gas internal energy [J]
global Tgas;           % Gas temperature
global ProjSpinRate;   % Spin Rate rotations/s
global RecoilX;        % Recoil movement of gun [m]
global RecoilV;        % Recoil velocity [m/s]
global RecoilA;        % Recoil acceleration  [m/s/s]
global HeatEnergyLoss; % Heat energy lost to gub walls [J]

global FrictionEnergyLoss;

% 1x1 Variables
global nDerivitives;       % Number of differentials (i.e. acceleration,
velocity, burn rate, etc)
global Derivative;         % Array of differentials
global Integral;           % Array of integrals
```

```
global Ign_FlameTemp;       % Igniter Flame Temperature [K]
global Ign_Mass;            % Igniter Mass [kg]
global Ign_Fp;              % Force constant [J/kg]
global Ign_R;               % Ign Gas Constant [J/kg.K]
global Ign_CoVol;           % Ign gas co volume [cc/g]
global Ign_Gamma;           % Ign gas gamma value
global Ign_Cv;              % (calculated value) Ign gas spec heat capacity
at constant volume [J/kg.K]
global Ign_Cp;              % (calculated value) Ign gas spec heat capacity
t constant pressure [J/kg.K]

global nProps;              % Number of Propellants (Input)
global PropGeom;            % Not used in air gun model (Input)
PropGeom =
struct('Type',0,'a',0.0,'b',0.0,'c',0.0,'L',0.0,'D',0.0,'P1',0.0,'P2',0.0,'
SlabW',0.0,'SlabL',...
                   0.0,'SlabT',0.0,'SlotW',0.0);
global PropChem;            % Gas properties (Input)
PropChem =
struct('R',0.0,'Cv',0.0,'Cp',0.0,'Fp',0.0,'CoVol',0.0,'FlamTemp',0.0,'Rho',
0.0,'Gamma',...
                   0.0,'Mass',0.0,'BurnCoeff',0.0,'BurnExp',0.0);
global GrainVolume;         % Propellant Grain volume (2D array for each
propellant and cycle)
global GrainVolume0;
global GrainArea;
global GrainArea0;
global NormGrainArea;       % Normalized Grain Area (2D array for entire
cycle and each propellant)
global nGrains;
global grainDis;

global nBins;
global PDFSim;              % On(1) - use single value or off(0)-use
distribution

% Input Data
%%%%%%%%%%%%%%%%%%%%%%%%%%%%%%%%%%%%%%%%%%%%%%%%%%%%%%%%%%%%%%%%%%%%%%%%%%%
%%%%%%%%%%%%%%%%%%%%%%%%%%%%%%%%%%%%
% Assign input parameters of Gun
% Gun Input (12.7)
ChVolume = 30;                                  %
ChVolume = ChVolume/1000000;                      % Chamber Volume [mm3] to [m3]
ProjMass = 42.0/1000.0;                           % ProjMass[kg]
GrooveLength =(915-(40+63.124))/1000;             % [m]
RiflingTwist = 7;                                 % Double chech 1x360deg (2pi
radians) Rotation in this number of calibres travel [rad/m]
RecoilMass = 0.0;                                 % Total mass of recoil - in
this case the rifle - free recoil - if mass = 0, recoil is ignored
RecoilResistance0 = 0.0;                          % Initial threshold recoil
resistance [N]
RecoilResistance = 0.0;                           % Cycle Recoil resistance  [N]
GrooveDiam =   12.941/1000.0;                     % [m]
LandDiam = 12.687/1000.0;                         % [m]
GLRatio = 1.7102;                                 % Ratio of groove width to
land width
BarrelDiamSq = LandDiam*GrooveDiam;
% Resistance Model
XR(1) = 0.0;                    % [m]
XR(2) = 0.010;                  % Half of drive band width
```

```
XR(3) = 0.015;                  % Full Drive band width
XR(4) = GrooveLength;           %
PR(1) = 1;                      % Initial Resistance Pressure - Shot Start
[MPa]
PR(2) = 15.0;                   % Further resistance values [MPa]
PR(3) = 0.01;
PR(4) = 0.01;
% Fitting factors (STANAG)
Fbr = 1.00;                      % (Input) Bore resistance factor
Fr  = 1.00;                      % (Input) Burn Rate adjustment factor
Fft = 1.0;                       % (Input) Force constant temperature
factor
Ft  = 1.0;                       % (Input) Burn rate temperature factor


% Heat Loss Input values
h0 = 11.35;                      % (Input) Heat Transfer Coeff of air [W/m2
K]
WallThickness = 2.0/1000;        % (Input) Nominal wall thickness [m]
CpWall    = 460.28;              % (Input) Wall material heat capacity
[J/kg K]
RhoWall   = 8020.1;              % (Input) Wall material density [kg/m3]
WallT0    = 300.0;               % (Input) Wall initial temperature
fFriction = 1.0;                 % (Input) Wall Preheat factor

% Ignition gas properties (All Ignition gas is released at t0)
% Black powder nominal values
Ign_Mass  = 0.09/1000;              % [kg]
Ign_Fp    = 303.3*1000.0;           % Force constant [J/kg]
Ign_CoVol = 0.636/1000;             % Ign gas co volume [cc/g]
Ign_Gamma = 1.3561;                                     % Ign gas gamma
value
Ign_FlameTemp = 3863.0;                                 % Combustion
flame temperature [K]
Ign_Cv = Ign_Fp/((Ign_Gamma-1)*Ign_FlameTemp);          % Ign gas spec
heat capacity cv constant volume [J/kg.K]
Ign_Cp = Ign_Fp*Ign_Gamma/((Ign_Gamma-1)*Ign_FlameTemp);    % Ign gas spec
heat capacity cp constant pressure [J/kg.K]
Ign_R = Ign_Fp/Ign_FlameTemp;                           % Ign Gas
Constant [J/kg.K]

% Propellant is solid propellant grains
nProps = 1;

% Propellant 1 Input
% Thermochemical and burn rate
PropChem.Mass(1)      = 16/1000;            % kg
PropChem.Fp(1)        = 934.3*1000.0;       % J/kg
PropChem.CoVol(1)     = 1.048/1000;         % m3/kg
PropChem.FlameTemp(1) = 2586.1 ;            % K
PropChem.Gamma(1)     = 1.2584;             %
PropChem.Rho(1)       = 1.569*1000.0;       % kg/m3
PropChem.Cv(1) = Fft*PropChem.Fp(1)/((PropChem.Gamma(1) -
1)*PropChem.FlameTemp(1));                   % J / (kg K)
PropChem.Cp(1) = Fft*PropChem.Fp(1)*PropChem.Gamma(1)/((PropChem.Gamma(1) -
1)*PropChem.FlameTemp(1));

PropChem.R(1)  = Fft*PropChem.Fp(1)/PropChem.FlameTemp(1);
```

The required inputs inserted via IB simulation model to simulate a basic gun IB cycle according to STANAG 4367 (Edition 2) for 5.56 mm (adapted from RDM IB simulation codes):

```
clc;
clear all;
close all;

% Global Data Definition Section
% Gun and projectile parameters
global ChVolume;                    % (Input) Chamber nett volume
global ProjMass;                    % (Input) Projectile Mass
global GrooveLength;                % (Input)
global GrooveDiam;                  % (Input)
global LandDiam;                    % (Input)
global GLRatio;                     % (Input)
global BarrelDiamSq;                % Calculated according to STANAG
global RiflingTwist;                % (Input)1 360deg Rotation in Number of
calibres (Input)
global RecoilMass;                  % (Input) Recoil part total mass  (Input)
global RecoilResistance0;           % (Input) Initial threshold recoil
resistance [N]  (Input)
global RecoilResistance;            % (Input) Cycle Recoil resistance [N]
(Input)
global XR;                          % (Input) Resistance model - x    [m]
(Input)
global PR;                          % (Input) Resistance model - Pr   [MPa]
(Input)
global Presist;

% STANAG adjustment factors
global Fbr;                         % (Input) Bore resistance factor
global Fr;                          % (Input) Burn Rate adjustment factor
global Fft;                         % (Input) Force constant temperature
factor
global Ft;                          % (Input) Burn rate temperature factor

% Heat Loss Input values
global h0;                          % (Input) Heat Transfer Coeff of air
global WallThickness;               % (Input) Nominal wall thickness
global CpWall;                      % (Input) Wall material heat capacity
global RhoWall;                     % (Input) Wall material density
global WallT0;                      % (Input) Wall initial temperature
global TWall;                       % (Input) Wall initial temperature
global fFriction;                   % (Input) Wall Preheat factor

% State Vector arrays (1xn variables)
global TimeStep;        % Time step size (Input)
global Time;            % Cycle Time in [s]
global Z;               % Propellant fraction burnt for each propellant and
entire cycle(2d array) - 1st index:cycle no, 2nd index: propellant no
global BurnDist;        % Propellant Burn Distance vector (for each
propellant)
global BurnRate;        % Propellant Burn Rate (for each propellant)
global X;               % Projectile position [m]
global V;               % Projectile velocity [m/s]
```

```
global A;              % Projectile accelleration [m/s/s]
global Pbr;            % Breech Pressure
global Pc;             % Chamber average pressure
global Pba;            % Projectile Base Pressure
global Egas;           % Gas internal energy [J]
global Tgas;           % Gas temperature
global ProjSpinRate;   % Spin Rate rotations/s
global RecoilX;        % Recoil movement of gun [m]
global RecoilV;        % Recoil velocity [m/s]
global RecoilA;        % Recoil accelleration  [m/s/s]
global HeatEnergyLoss; % Heat energy lost to gub walls [J]

global FrictionEnergyLoss;

% 1x1 Variables
global nDerivitives;       % Number of differentials (i.e. acceleration,
velocity, burn rate, etc)
global Derivative;         % Array of differentials
global Integral;           % Array of integrals

global Ign_FlameTemp;      % Igniter Flame Temperature [K]
global Ign_Mass;           % Igniter Mass [kg]
global Ign_Fp;             % Force constant [J/kg]
global Ign_R;              % Ign Gas Constant [J/kg.K]
global Ign_CoVol;          % Ign gas co volume [cc/g]
global Ign_Gamma;          % Ign gas gamma value
global Ign_Cv;             % (calculated value) Ign gas spec heat capacity
at constant volume [J/kg.K]
global Ign_Cp;             % (calculated value) Ign gas spec heat capacity
t constant pressure [J/kg.K]

global nProps;             % Number of Propellants (Input)
global PropGeom;           % Not used in air gun model (Input)
PropGeom =
struct('Type',0,'a',0.0,'b',0.0,'c',0.0,'L',0.0,'D',0.0,'P1',0.0,'P2',0.0,'
SlabW',0.0,'SlabL',...
                  0.0,'SlabT',0.0,'SlotW',0.0);
global PropChem;           % Gas properties (Input)
PropChem =
struct('R',0.0,'Cv',0.0,'Cp',0.0,'Fp',0.0,'CoVol',0.0,'FlamTemp',0.0,'Rho',
0.0,'Gamma',...
                  0.0,'Mass',0.0,'BurnCoeff',0.0,'BurnExp',0.0);
global GrainVolume;        % Propellant Grain volume (2D array for each
propellant and cycle)
global GrainVolume0;
global GrainArea;
global GrainArea0;
global NormGrainArea;      % Normalized Grain Area (2D array for entire
cycle and each propellant)
global nGrains;
global grainDis;

global nBins;
global PDFSim;             % On(1) - use single value or off(0)-use
distribution

% Input Data
%%%%%%%%%%%%%%%%%%%%%%%%%%%%%%%%%%%%%%%%%%%%%%%%%%%%%%%%%%%%%%%%%%%%%%%%%%%
%%%%%%%%%%%%%%%%%%%%%%%%%%%%%%%%%%%%
```

```
% Assign input parameters of Gun
% Gun Input (5.56)
ChVolume = 3.0/1000000;                 % Chamber Volume [mm3] to [m3]
ProjMass = 4.1/1000.0;                          % ProjMass[kg]
GrooveLength = 461.5/1000;                      % [m]    461.5
RiflingTwist = 7;                               % 1x360deg (2pi radians)
Rotation in this number of calibres travel [rad/m]
RecoilMass = 0.0;                               % Total mass of recoil - in
this case the rifle - free recoil - if mass = 0, recoil is ignored
RecoilResistance0 = 0.0;                        % Initial threshold recoil
resistance [N]
RecoilResistance = 0.0;                         % Cycle Recoil resistance
[N]
GrooveDiam = 5.69/1000.0;                       % [m]
LandDiam = 5.56/1000.0;                         % [m]
GLRatio = 1.7102;                               % Ratio of groove width to
land width
BarrelDiamSq = LandDiam*GrooveDiam;

% Fitting factors (STANAG)
Fbr = 1.0;                        % (Input) Bore resistance factor
Fr  = 1.0;                        % (Input) Burn Rate adjustment factor
Fft = 1.0;                        % (Input) Force constant temperature
factor
Ft  = 1.0;                        % (Input) Burn rate temperature factor

% Heat Loss Input values
h0 = 11.35;                       % (Input) Heat Transfer Coeff of air [W/m2
K]
WallThickness = 2.0/1000;         % (Input) Nominal wall thickness [m]
CpWall    = 460.28;                  % (Input) Wall material heat capacity
[J/kg K]
RhoWall   = 8020.1;                % (Input) Wall material density [kg/m3]
WallT0    = 300.0;                  % (Input) Wall initial temperature
fFriction = 1.0;                  % (Input) Wall Preheat factor

% Resistance Model
XR(1) = 0.0;                     % [m]
XR(2) = 0.0005;                   % Half of drive band width
XR(3) = 0.001;                   % Full Drive band width
XR(4) = GrooveLength;            %
PR(1) = 1;                       % Initial Resistance Pressure - Shot Start
[MPa]
PR(2) = 19.0;                    % Further resistance values [MPa]
PR(3) = 16;
PR(4) = 16;

% Ignition gas properties (All Ignition gas is released at t0)
% Black powder nominal values
Ign_Mass  = 0.02/1000;              % [kg]
Ign_Fp    = 303.3*1000.0;           % Force constant [J/kg]
Ign_CoVol = 0.636/1000;             % Ign gas co volume [cc/g]
Ign_Gamma = 1.3561;                                     % Ign gas gamma
value
Ign_FlameTemp = 3863.0;                                 % Combustion
flame temperature [K]
Ign_Cv = Ign_Fp/((Ign_Gamma-1)*Ign_FlameTemp);          % Ign gas spec
heat capacity cv constant volume [J/kg.K]
Ign_Cp = Ign_Fp*Ign_Gamma/((Ign_Gamma-1)*Ign_FlameTemp);    % Ign gas spec
heat capacity cp constant pressure [J/kg.K]
```

```
Ign_R = Ign_Fp/Ign_FlameTemp;                                    % Ign Gas
Constant [J/kg.K]

% Propellant is solid propellant grains
nProps = 1;

% Propellant 1 Input
% Thermochemical and burn rate
PropChem.Mass(1)      = 1.7/1000;           % kg
PropChem.Fp(1)        = 1028.3*1000.0;       % J/kg
PropChem.CoVol(1)     = 1.016/1000;          % m3/kg
PropChem.FlameTemp(1) = 2980.0 ;             % K
PropChem.Gamma(1)     = 1.2417;              %
PropChem.Rho(1)       = 1.592*1000.0;        % kg/m3
PropChem.Cv(1) = Fft*PropChem.Fp(1)/((PropChem.Gamma(1) -
1)*PropChem.FlameTemp(1));                    % J / (kg K)
PropChem.Cp(1) = Fft*PropChem.Fp(1)*PropChem.Gamma(1)/((PropChem.Gamma(1) -
1)*PropChem.FlameTemp(1));
PropChem.R(1)  = Fft*PropChem.Fp(1)/PropChem.FlameTemp(1);
```

Important equations used in IB simulation for both 12.7 mm and 5.56 mm adapted from RDM IB simulation Codes (Step) according to STANAG:

```
function Step2(n,i,dt)
% Function to perform one time step integration (forward Euler)
% i is step number
% dt is time step size in [s]
% Global arrays to be updated
global Time;
global Integral;
global Derivitive;
global PropMass;
   CalcIBState(i);
  % Integrate the burn rate to yield burn distance
  for j=1:n
    Integral(j) = Derivative(j)*dt + Integral(j);
  end

  % Advance Time
    Time(i) = Time(i-1) + dt;
end


function CalcIBState(i)
% Function to calculate current IB state at start of time step
% Determine Derivatives to be integrated from here
%
```

```
global CVVolume;
global BurnDist;
global Derivitive;
global Integral;
global BurnRate;
global GrainVolume0;
global Z;
global GasMass;
global Pressure;
global Vol;
global PropChem;
global PropGeom;
global GrainArea;
global nGrains;
global grainDis;
global nBins;
global PropMass;
global Distribution;
% Get integrated values
BurnDist(i) = Integral(1);

% Calculate propellant combusted as result of propellant burnt at start of
% time step

if Distribution (proposed method)
  % For probability distribution method
distrVolume     = 0.0;
totalVolume     = 0.0;
totalSurface    = 0.0;
totalPropMass = 0.0;

 for j = 1:nBins
    PropGeom.D              = grainDis(j,1);
% Grain diameter ??
    [GrainVolume GrainArea(i)] = Form(BurnDist(i),PropGeom);
    totalVolume             = totalVolume + grainDis(j,4)*GrainVolume;
% grainDis(j,2) = probability
    totalSurface            = totalSurface + grainDis(j,4)*GrainArea(i);
 end
 else
  % For traditional single value method (RDM Method)
    [GrainVolume, GrainArea] = Form(BurnDist,PropGeom);
% Single value
    totalVolume              = nGrains * GrainVolume;
end

GrainVolume = totalVolume;
Vol(i) = totalVolume;
GrainArea(i) = totalSurface;

Z(i) = 1.0 - GrainVolume/GrainVolume0;
GasMass(i) = Z(i)* PropChem.PropMass(1);


% Calculate pressure from Nobel Abel State Equation
Pressure(i) = 101000.0...               % Atmospheric Pressure
              + GasMass(i)*PropChem.PropFp(1)/(CVVolume - ...
              PropChem.PropMass(1)*(1-Z(i))/(PropChem.PropRho(1))-
GasMass(i)*...
```

```
            PropChem.PropCoVol(1);

% Determine burn rate based on pressure
BurnRate(i) = PropChem.PropBurnCoeff(1) *
(Pressure(i)/1000000.0)^PropChem.PropBurnExp(1);  % mm/s , Pressure should
be in MPa

% Set Derivatives new burn rate for this time step to integrate for the
next step
Derivative(1) = BurnRate(i)/1000.0;
% derivative in m/s

end
```